DUAL ISOLATION FOR ENHANCED SEISMIC PROTECTION

DUAL ISOLATION FOR ENHANCED SEISMIC PROTECTION

By

ASHKAN EZAZI, M.Sc., B.Sc.

A Thesis

Submitted to the School of Graduate Studies

in Partial Fulfilment of the Requirements for the Degree

Master of Applied Science

McMaster University

© Copyright by Ashkan Ezazi, July 2015

MASTER OF APPLIED SCIENCE (2015) McMaster University
Hamilton, Ontario

TITLE: Dual Isolation for Enhanced Seismic Protection

AUTHOR: Ashkan Ezazi, B.Sc., Hamadan Institute of Higher Education, M.Sc., Mazandaran University, Iran

SUPERVISOR: Dr. Tracy Becker

NUMBER OF PAGES: xii, 67

To My Mom and Dad

&

My Beloved Sister

Abstract

Base isolated buildings are well known to provide enhanced performance due to minimized accelerations and decreased interstory drifts. However, the reduced demands are obtained at the expense of large displacements at the isolation layer. This study investigates an innovative system, termed ‘dual isolation’, which applies two layers of isolation, one at the base and one mid-story to resolve this issue. An analytical solution for the equation of motion of the proposed system is developed based on linear isolation theory. This creates a foundation to assess the behavior of various types of seismic protection systems and to select the damping, mass and frequency ratio that leads to an optimal dual isolation design. Time history responses of the dual isolation system with viscous damping are compared to those of a conventional isolation counterpart to examine the effectiveness of the system. The system reduces first floor displacements by 40% on average, while the roof displacement is increased by roughly 15%. This results in reduced design forces for the structure. In addition, accelerations, especially above the second isolation layer, are significantly decreased. By reducing story shears and accelerations, the dual isolation system limits damage to both structural and nonstructural systems and components, thereby increasing global system performance.

Acknowledgements

I am deeply grateful to my supervisor, Dr. Tracy Becker, for her continuous support and patient guidance throughout my studies.

I would like to thank my committee members, Dr. Michael J. Tait, Dr. A. Ghani Razaqpur.

I would also like to acknowledge Dr. Vladimir Mahalek and Dr. Dimitrios Konstantinidis for insightful comments and encouragements.

Lastly I would like to thank Joanne Gadawski, Carol Robinson, Dulcie Amaral and Richard Allen for all their help.

Table of Contents

List of Figures

List of Tables

1- Introduction

The idea of decoupling a structure from horizontal earthquake motions is made possible by placing base isolation devices at the interface of a structure and its foundation. To date there are over 3000 isolated buildings in Japan, over 200 in United States and many more in over 30 earthquake-prone countries (Wolff et al., 2014). The application of base isolation has been successful and if used more widely, holds a great potential to save lives and prevent costly damage caused by either high floor acceleration or large story drifts.

In classic isolation systems, in which the isolation layer is located at the base of a building, the reduction in the imposed accelerations to the structure is obtained at the expense of large displacements at the isolation layer. To meet this displacement demand, designers must provide large isolation gaps. These gaps may not be possible in densely populated areas and can increase the total project cost when real estate is highly valuable. Therefore, this may create a barrier against applications of base isolation. This problem is a continuous trade-off; if smaller floor accelerations are desired in order to achieve a required performance objective, displacements must be further increased.

This study aims to reduce the displacement of the base isolation level by applying an additional layer of isolation at mid story. The combined system is referred to as 'dual isolation.' The dual isolation approach bears similarities to both traditional isolation and tuned mass damper (TMD) theory, therefore the theory of these systems is studied to provide valuable insight for the practical design of the dual isolation system. Using simplified models, an analytical investigation of the structure is conducted to better explain the dual isolation system behaviour, and select optimal design parameters. The performance of a multi degree of freedom (DOF) dual isolation system and the acceleration demands on building systems and components are then compared to classic base isolation under a suite of ground motions with various frequency content. In addition, the sensitivity of the system to soil conditions and design parameters is

investigated, validating the stable behaviour of the system under a wide range of design parameters and ground inputs. If optimized, the dual isolation system offers large reduced demand parameters, and can be used for applications which call for enhanced protection of the building systems and components.

1-1- Review of Classic Base Isolation

In classic base isolation a layer of low lateral stiffness is placed between structure and foundation to change the mode shape and reduce the accelerations transmitted to the structure (Naeim and Kelly, 1999). Base isolation lengthens the building's natural period and thus, reduces the accelerations of the first mode as shown in Fig. 1-1. The first dynamic mode of the isolated structure is altered from traditional fixed base buildings, and involves deformation only in the isolation system while the superstructure (the structure above the isolation layer) will act as a nearly rigid body (Fig. 1-2).

The role of higher modes are minimal in base isolation, because the flexible layer of isolation systems filters high-frequency energy and prevents its transmission throughout the superstructure (Becker and Mahin, 2012). A study by Sakamato (1978) suggested that interstory drifts and inertial forces due to the absolute accelerations are the major cause of

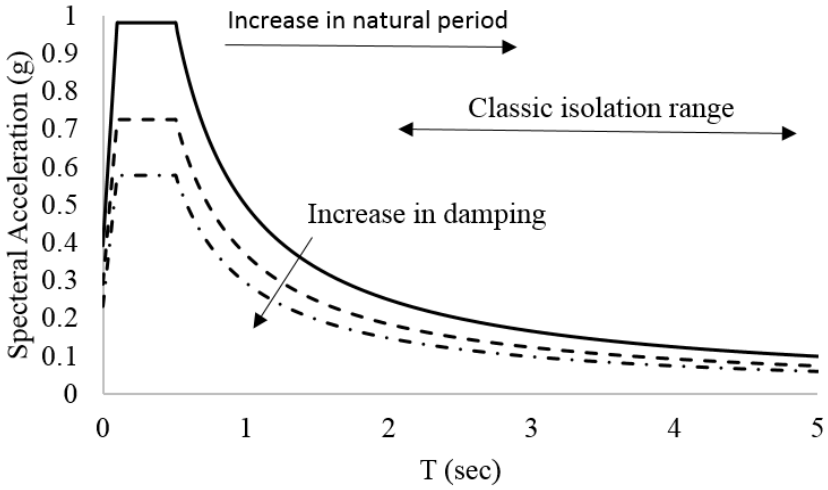

Figure 1-1: Effect of base isolation on spectral acceleration

damage to building systems and contents. To protect the building contents as well as protecting the primary structural system, the use of seismic isolation devices was proposed by Kelly (1982) through an experimental study of a five story frame supported on rubber bearings. For an average of 8 ground motions, the findings showed 60% reduction in peak floor accelerations of a fixed base building. Moreover, it was shown that while the acceleration demands on building contents can be up to 10 times higher than ground acceleration for fixed base buildings, the transmitted accelerations in base isolated frames were greatly decreased by an order of 3 to 10.

Figure 1-2 shows the lateral displacement of fixed and base isolated structures. Because the isolation system absorbs the deformation, the superstructure displaces as a rigid body. This behaviour prevents the loss of nonstructural architectural and mechanical systems such as heating-ventilation-air-conditioning (HVAC) systems, elevators, light fixtures and suspended ceilings and protects acceleration sensitive contents such as furniture, computer systems, power generator systems, etc. (Reinoso and Miranda, 2005).

Increasing the isolation period leads to large displacements as shown in Fig.1-3, this is a continuous tradeoff between accelerations and displacement demands for base isolation systems under presence of long duration pulses.

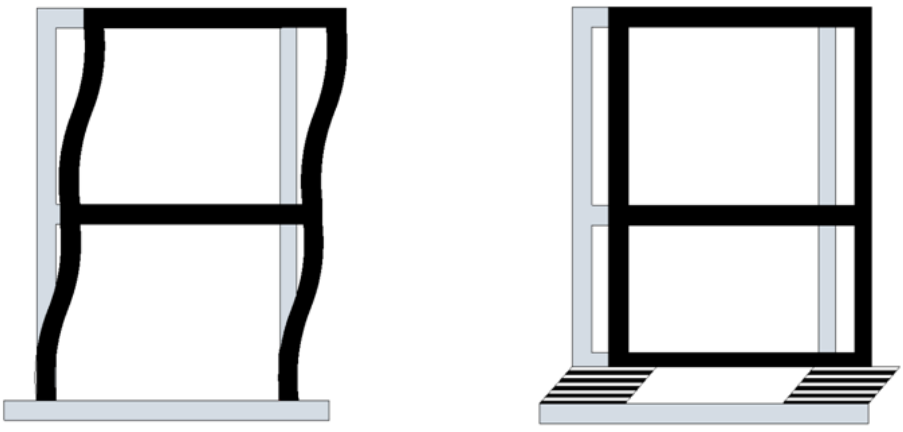

Figure 1-2: Lateral deformation of fixed base and base isolated buildings

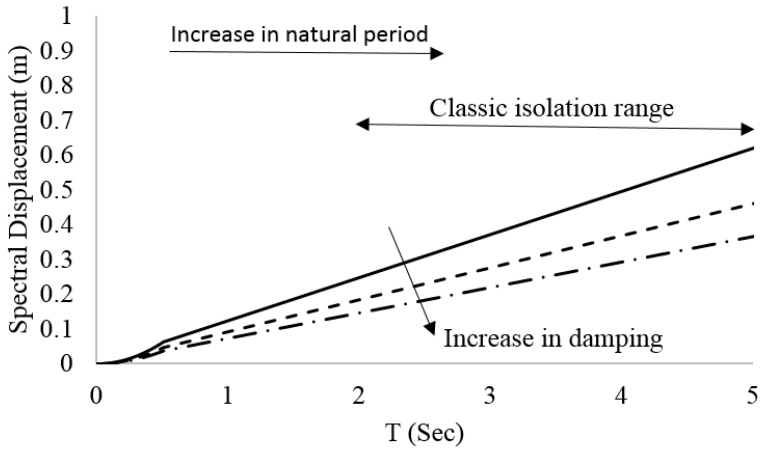

Figure 1-3: Effect of base isolation on displacement demand

Jangid and Kelly (2001) showed that these pulses have significant impact on displacement of isolation layer when the period of the isolation system approaches the pulse period. Thus, isolated structures in areas prone to pulse-type motions require larger space to their adjacent buildings than other type of conventional structures to adequately accommodate the maximum displacement of the two buildings.

According to ASCE 7- 05; the minimum moat wall clearance is considered equal to the maximum displacement at the base level under maximum considered earthquake (MCE). Considering the required space for the clearance gap and moat walls in addition to the cost of the concrete moat walls and moat cover significantly increases the construction costs especially in large cities, where real estate is highly valuable.

One approach for decreasing displacements in isolation systems is to incorporate supplementary damping to the system through mechanical dampers as shown in Fig. 1-4. Although controlling the isolator displacement by additional damping is effective, it can increase floor acceleration and story drifts in the superstructure. The dampers drive energy into higher modes, increase their responses and negate the effect of base isolation. Furthermore, supplementary damping increases the chance that base isolation system does not displace in lower level earthquakes (Kelly, 1999).

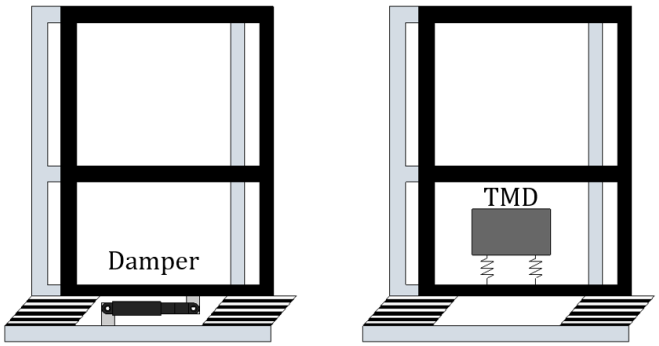

Figure 1-4: Incorporating additional damping and vibration absorbers to control the displacement of base isolation systems

Wolff et al., (2014) showed that for highly damped isolations (effective damping of 20-30%) the addition of damper devices leads to a general increase in drifts and shear forces of base isolated buildings, however for low damped bearings this addition results in reduction in displacement demand without having detrimental effect on floor accelerations and story drifts.

1-2- Review of Previously Proposed Isolation Schemes

The most common isolation configuration is to install a diaphragm immediately above and below the isolation layer which permits earthquake loads to be distributed to the isolators according to their stiffness.

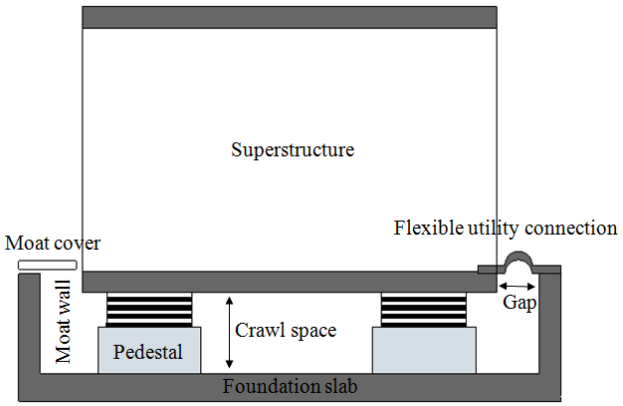

Figure 1-5: Components of a base isolation system

A crawl space is usually considered at the isolation level to allow frequent inspections, in addition; the design scheme should not restrain the relative horizontal displacement of the isolation system, the superstructure, and the nonstructural systems at the interface of isolation layers. A schematic representation of the isolation system components are shown in Fig. 1-5. For a building without a basement, the isolator is mounted on a foundation pad and structure constructed above them. If the building has a basement then the isolator can be installed at the top, bottom or mid-height of the basement columns and walls (Kelly, 2001).

Self-mass dampers and mid-story isolation systems are two new trends in research programs. Mid-story isolation divides the building into two parts at an interface layer located somewhere above the first floor, has been employed as a solution that allows real-state to be added to an existing structure without significantly increasing the lateral force demands in the existing structures (Dutta et al., 2008). It is also used for new construction as a system to reduce structural demands and facilitate the transition between two structural systems (Tsuneki et al., 2008). Mid-story isolation, implemented at any level, is effective in reducing the force demand and story drifts above the isolation layer. In theory, the substructure is a fixed base building with a TMD with large mass ratio, and thus the system could be designed to reduce demands below the isolation layer as well. However, Ryan and Earl (2010) found mid-story isolation was minimally effective in mitigating the lower level responses compared to base isolation for earthquake excitation. One example of using such systems is the Iidabashi First Building in Japan. Here, the lower levels are made of steel and the upper levels are reinforced concrete structure (Elangi, 2008). Another example is the Swatch Group's building in Japan, with four isolation layer at mid-stories, here, considering each portion of the building as a large mass damper the seismic forces are reduced by 38% compared to a fixed base structure (Kidokora, 2008).

Chien Pan et al., 1995 introduced the concept of multi-layer isolation (more than two layers) to improve the effectiveness of base isolation in tall buildings. They numerically

investigated a 16 story structure divided into four segments under the El Centro ground motion and observed a 37% decrease in base displacement while maintaining structural accelerations similar to a classic base isolated case. Later, Chien Pan and Cui (1998) studied the response of the same structure under random excitation. For stiff soil conditions they found 46% reduction in base displacements using four isolation layers. In 2010, Ryan and Earl studied the displacement demand in a six story building with multiple isolation layers varying the locations of the isolation systems. Numerical results showed roughly 30% reduction in base displacement and 30% increase in roof displacement in the system with two isolation layers located at the base and mid-height compared to a classic base isolated model. However, the location and properties of the isolation layers were not optimized, and the potential for reducing floor accelerations was not considered.

1-3- Review of Tuned Mass Dampers (TMD)

The tuned mass damper is a mechanical device used to mitigate unwanted vibration. In its simple form, a TMD includes one spring and a mass that is attached to a single degree of freedom system, as shown in Fig. 1-6. TMDs are usually installed at the top floor of a fixed base building and the frequency is tuned to the fundamental mode of the structure. These vibration absorbers have been successfully applied to mitigate wind or traffic induced vibration of buildings by reducing the displacement demands and increasing the overall damping of the main structure since 1970s (Chen and Wu, 2001).

Although TMDs are effective for low level excitations, studies have shown limited effectiveness in reducing maximum response under seismic loading (Chowdhury and Iwuchnkwu, 1987, Clark, 1988 and Sladek and Klinger, 1983). The seismic performance of TMDs is dependent on ground motion properties. While they are effective for narrow band, long duration earthquakes, they did not reduce the peak response in pulse-type ground motions (Matta, 2013).

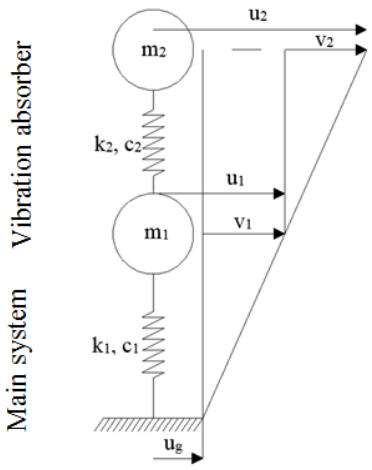

Figure 1-6: Tuned mass damper

There are mainly two reasons for this performance. First, earthquake loads are typically impulsive and reach the maximum values rapidly, while TMDs are not set into significant motion yet in such a short period, therefore they do not absorb the induced energy as expected. Second, Earthquake motions with wide spectrum of frequency components induce vibration in not only the fundamental mode, but also higher modes of buildings. Thus, a TMD which is tuned to the fundamental frequency is not able to reduce the total response of the structure (Chen & Wu, 2001).

Studies utilizing TMDs for the reduction of isolated building response have similar trends. Palazzo and Petti (1999) and Taniguchi et al. (2008) investigated the performance of a base isolated system with TMDs added to control the displacement demand. Both studies found that the TMD efficacy decreases as the damping ratio of the isolators increases. Taniguchi et al. (2008) showed that TMDs located directly above the isolation layer can reduce the displacement demand of lightly damped (below 10%) base isolated structures by up to 25% for white noise and far field excitations.

2- Theoretical Basis

2-1- Linear Theory

The theory for the dual isolation system is based on classic linear isolation theory, given in Naeim and Kelly (1999), which is based on a two DOF structural model with one DOF representing the isolation layer with period T_1 and damping ratio of β_1 and the second DOF representing the superstructure with period T_2 and damping ratio of β_2 as shown in Fig. 2-1. Simplifications based on the assumption that the nominal frequency of the superstructure ω_2, is significantly larger than the nominal frequency of the isolation layer ω_1, are used to gain insight into the system behaviour. In Fig. 2-1, m_1 and m_2 represent the mass of first and second DOFs respectively. The absolute displacements of the two masses are shown by u_1 and u_2, however the relative displacements (v_1 and v_2) are used for following calculations. The relative displacement of the first and second DOFs are

$$v_1 = u_1 - u_g, \;\; v_2 = u_2 - u_1 \qquad 2\text{-}1$$

where u_g is the ground displacement. The nominal frequencies are

$$\omega_1 = \sqrt{\frac{k_1}{(m_1 + m_2)}}, \; \omega_2 = \sqrt{\frac{k_2}{m_2}} \qquad 2\text{-}2$$

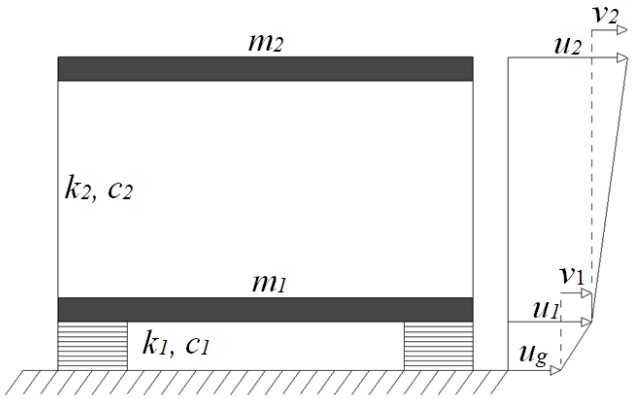

Figure 2-1: Parameters of classic isolation system (2DOF model)

The damping ratios β_1 and β_2 are given by

$$\beta_1 = \frac{c_1}{2(m_1+m_2)\omega_1},\ \beta_2 = \frac{c_2}{2m_2\,\omega_2} \tag{2-3}$$

In which c_1 and c_2 are the viscous damping coefficients of the first and second DOFs. The equation of motion for the new system can be written as

$$(m_1 + m_2)\ddot{v}_1 + m_2\ddot{v}_2 + c_1\dot{v}_1 + k_1 v_1 = -(m_1 + m_2)\ddot{u}_g \tag{2-4}$$

$$m_2\ddot{v}_1 + m_2\ddot{v}_2 + c_2\dot{v}_2 + k_2 v_2 = -m_2\ddot{u}_g \tag{2-5}$$

Introducing $M = m_1 + m_2$, the equations of motion can be written in matrix notation as

$$\begin{bmatrix} M & m_2 \\ m_2 & m_2 \end{bmatrix}\begin{Bmatrix} \ddot{v}_1 \\ \ddot{v}_2 \end{Bmatrix} + \begin{bmatrix} c_1 & 0 \\ 0 & c_2 \end{bmatrix}\begin{Bmatrix} \dot{v}_1 \\ \dot{v}_2 \end{Bmatrix} + \begin{bmatrix} k_1 & 0 \\ 0 & k_2 \end{bmatrix}\begin{Bmatrix} v_1 \\ v_2 \end{Bmatrix} = \begin{bmatrix} M & m_2 \\ m_2 & m_2 \end{bmatrix}\begin{Bmatrix} 1 \\ 0 \end{Bmatrix}\ddot{u}_g \tag{2-6}$$

The mass ratio γ is defined as

$$\gamma = \frac{m_2}{m_1 + m_2} = \frac{m_2}{M} \tag{2-7}$$

Dividing Eq. 2-4 by M and Eq. 2-5 by m_2 will give

$$\ddot{v}_1 + \gamma\ddot{v}_2 + 2\omega_1\beta_1\dot{v}_1 + \omega_1^2 v_1 = -\ddot{u}_g \tag{2-8}$$

$$\ddot{v}_1 + \ddot{v}_2 + 2\omega_2\beta_2\dot{v}_2 + \omega_2^2 v_2 = -\ddot{u}_g \tag{2-9}$$

Solving the characteristic equation for ω_n, the fundamental frequencies are defined as

$$w_n{}^{*2} = \frac{\omega_1^2 + \omega_2^2 \pm (\omega_1^4 + \omega_2^4 + (-2 + 4\gamma)\omega_1^2\omega_2^2)^{\frac{1}{2}}}{2(1-\gamma)} \tag{2-10}$$

The model used by Kelly and Naeim, shown in Fig. 2-1, considers the superstructure as an independent degree of freedom, However this system can be estimated by a simpler analysis by treating the superstructure as rigid. The deformation of the superstructure is negligible when the period of the isolation system is much longer than the period of its superstructure; the combined behaviour of isolation layer and its superstructure can be considered as one degree of freedom with period of T_1 and damping ratio of β_1.

Extending the theory to the dual isolation system, using the simplified model, the performance of the dual isolation system is compared to the classic base isolation when each superstructure behaves as approximately rigid and the model can be defined as two DOF as shown in Fig. 2-2. The equations of motions derived above can then be used to model the dual isolation system.

The modal solutions are found for two cases: (1) where $\omega_2 > \omega_1$, representative of classic base isolation, and (2) where $\omega_1 > \omega_2$, representative of mid-story isolation, in which the period of the added isolation system is longer than the first layer.

2-1-1- Case 1 ($\omega_2 > \omega_1$)

For the case that the period of the first DOF is longer than the period of the second DOF, solving the Equation 2-10, the solution of the characteristic equation for the frequencies is

$$\omega_1^{*2} = \frac{(1-A)\omega_1^2}{2(1-\gamma)}, \qquad \omega_2^{*2} = \frac{2\omega_2^2 + (1+A)\omega_1^2}{2(1-\gamma)} \tag{2-11}$$

In Eq. 2-11, ω_1^* and ω_2^* are the natural frequencies of the first and second mode and A is a constant that is dependent on frequency ratio (ε) and mass ratio (γ) and truncated to ε^3.

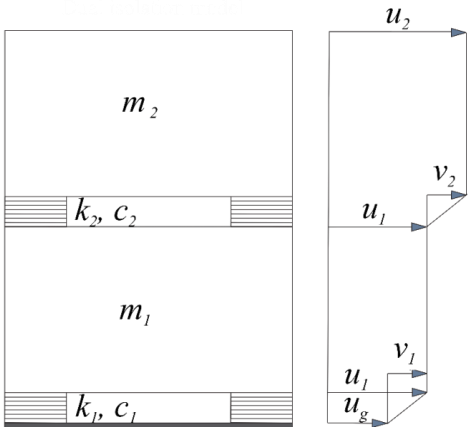

Figure 2-2: Parameters of the dual isolation system (rigid body assumption)

$$A = (-1 + 2\gamma) - 2(-\gamma + \gamma^2)\varepsilon + 2(\gamma - 3\gamma^2 + 2\gamma^3)\varepsilon^2 - 2(-\gamma + 6\gamma^2 - 10\gamma^3 + 5\gamma^4)\varepsilon^3 \quad (2\text{-}12)$$

Where ε is the frequency ratio

$$\varepsilon = \left(\frac{\omega_1}{\omega_2}\right)^2 \quad (2\text{-}13)$$

Truncating the constant *A* (Eq. 2-12) to ε^3gives good accuracy for the solution of Eq. 2-11 compared to numerical results as shown in Sec. 2-2. However there is loss in accuracy when both values of ε and γ approach to one. For example, the analytical solution for *A* has an error of 20% when $\varepsilon = 1$ and $\gamma = 0.7$. For classic base isolation and mid-story isolation in which the frequencies of each DOFs are well separated from each other this inaccuracy does not change the results, however for dual isolation system with $\gamma > 0.7$, although the calculated parameters are not accurate they are useful for the purpose of identifying the effects of design variables on systems performance.

Case 1 can be applied to represent the behaviour of classical isolation system in which the period of the first floor is well separated from the period of the second floor ($\omega_2 >> \omega_1$), and ε is on the order of 0.01. Using Eq. 2-11 for classic base isolation, and neglecting any terms higher than ε^2, natural frequencies are

$$\omega_1^{*2} = \omega_1^2(1 - \gamma\varepsilon)\,, \qquad \omega_2^{*2} = \frac{\omega_2^2}{1-\gamma}(1 + \gamma\varepsilon) \quad (2\text{-}14)$$

This is consistent with the solution that is offered by Kelly and Naeim (Naeim and Kelly, 1999). The classical modes of the combined system are denoted by ϕ^1 and ϕ^2, normalized modes are

$$\phi^1 = \begin{bmatrix} 1 \\ \dfrac{1 - 2\gamma + A}{\gamma(1 - A)} \end{bmatrix}, \qquad \phi^2 = \begin{bmatrix} 1 \\ \dfrac{(1 - 2\gamma - A)\varepsilon - 2}{\gamma((1 + A)\varepsilon + 2)} \end{bmatrix} \quad (2\text{-}15)$$

The mode shapes of two-DOF isolated system are shown in Fig. 2-3.

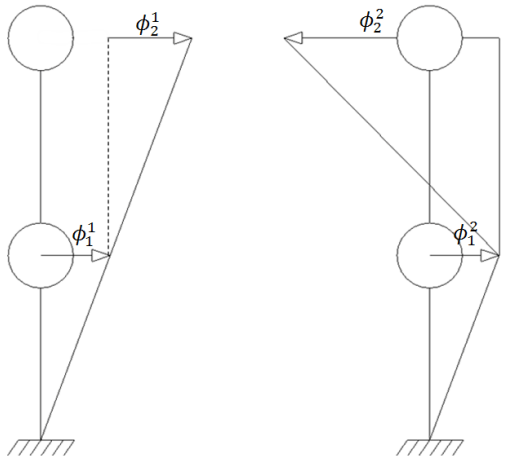

Figure 2-3: Mode shapes of the analytical model

The resulting modal participation factor, $L = \phi^T m\iota / \phi^T m\phi$ are

$$m = \begin{bmatrix} m_1 + m_2 & m_2 \\ m_2 & m_2 \end{bmatrix}, \qquad \iota = \begin{bmatrix} 1 \\ 0 \end{bmatrix} \tag{2-16}$$

$$L_1 = \frac{(-1+A)\gamma(-(1+A-2\gamma)m_2 + (-1+A)\gamma M)}{\left(1 + A^2(1-2\gamma) - 2\gamma + A(2-4\gamma+4\gamma^2)\right)m_2 + (-1+A)^2\gamma^2 M} \tag{2-17}$$

$$L_2 = \frac{\gamma(2+\varepsilon+A\varepsilon)(\gamma M(2+\varepsilon+A\varepsilon) + m_2(-2-(-1+A+2\gamma)\varepsilon))}{\gamma^2 M(2+\varepsilon+A\varepsilon)^2 + m_2((2+(-1+A)\varepsilon)^2 - 2\gamma(2+(1+A)\varepsilon)^2 - 4\gamma^2\varepsilon(2+A\varepsilon)}$$

2-1-2- Case 2 ($\omega_1 > \omega_2$)

For the case that the period of second DOF is longer than the first DOF, the modal natural frequencies are represented as

$$\omega_1^{*2} = \frac{(1-A)\omega_2^2}{2(1-\gamma)}, \qquad \omega_2^{*2} = \frac{2\omega_1^2 + (1+A)\omega_2^2}{2(1-\gamma)} \tag{2-18}$$

With A found in Eq. 2-12. However, the ratio between the two frequencies must now be expressed as $\varepsilon = \left(\frac{\omega_2}{\omega_1}\right)^2$, and the mode shapes are found as

$$\phi^1 = \begin{bmatrix} 1 \\ \dfrac{2(1-\gamma)-(1-A)\varepsilon}{\gamma(1-A)\varepsilon} \end{bmatrix}, \quad \phi^2 = \begin{bmatrix} 1 \\ \dfrac{-(1+A)\varepsilon-2\gamma}{\gamma((1+A)\varepsilon+2)} \end{bmatrix} \qquad 2\text{-}19$$

The resulting modal participation factors are 2-20

$$L_1 = \frac{(-1+A)\gamma\varepsilon(-1+A)\gamma M\varepsilon + m_2(-2+2\gamma+\varepsilon-A\varepsilon))}{(-1+A)^2\gamma^2 M\varepsilon^2 + m_2(4\gamma^2(1+(-1+A)\varepsilon)+(2+(-1+A)\varepsilon)^2 - 2\gamma(2+(-1+A)\varepsilon)^2}$$

$$L_2 = \frac{\gamma(2+\varepsilon+A\varepsilon)(\gamma M(2+\varepsilon+A\varepsilon)+m_2(-2-(-1+A+2\gamma)\varepsilon))}{\gamma^2 M(2+\varepsilon+A\varepsilon)^2 + m_2((2+(-1+A)\varepsilon)^2 - 2\gamma(2+(1+A)\varepsilon)^2 - 4\gamma^2\varepsilon(2+A\varepsilon)}$$

2-1-2-1- Mid Story Isolation

When the natural period of the second floor is much longer than the period of the first floor ($T_2 \gg T_1$) as in case 2, the model represents the behaviour of the mid-story isolation system. For mid-story isolation, the frequency ratio ε approaches zero and γ depends on the level at which the isolation interface is located. Eliminating ε^2 and higher, the mode shapes can be simplified from Eq. 2-19.

$$\phi^1 = \begin{bmatrix} 1 \\ \dfrac{1}{\gamma\varepsilon} \end{bmatrix}, \quad \phi^2 = \begin{bmatrix} 1 \\ -1+\varepsilon(\gamma-1) \end{bmatrix} \qquad 2\text{-}21$$

The resulting modal participation factors, $L = \phi^T m\iota / \phi^T m\phi$ are

$$L_1 = \frac{\gamma\varepsilon m}{m+2\gamma\varepsilon m} \qquad L_2 = \frac{M+m(-1+(-1+\gamma)\varepsilon)}{M-m} \qquad 2\text{-}22$$

The first mode participation factor L_1 depends on the frequency ratio; as ε approaches zero ($T_2 \gg T_1$) significant reduction in L_1 occurs. Thus, increasing the period of the

second DOF reduces the displacement demand on the first DOF, while increasing the demand on the second DOF as a result of increasing the first mode ϕ_2^1.

2-1-3- Base Isolation with Tuned Mass Damper

The behaviour of a tuned mass damped building is characterized by a small value of mass ratio γ and ε close to one. When ε approaches unity, the natural frequencies and mode shapes are determined from Case 1. It should be noted that approaching the procedures from Case 2 reaches to the same results. Because γ is small, eliminating the terms higher than γ^2 in Eq. 2-12 gives:

$$A = -1 + 8\gamma - 20\gamma^2 \tag{2-23}$$

Substituting *A* into Eq. 2-11 and setting $\omega_1 = \omega_2$ gives the natural frequencies,

$$\omega_1^{*2} = \frac{(1-4\gamma)\omega_1^2}{(1-\gamma)} \quad , \quad \omega_2^{*2} = \frac{(1+4\gamma)\omega_1^2}{(1-\gamma)} \tag{2-24}$$

The mode shapes are determined by substituting *A* and ε in Eq. 2-15,

$$\phi^1 = \begin{bmatrix} 1 \\ \dfrac{3-10\gamma}{1-4\gamma} \end{bmatrix} \sim \begin{bmatrix} 1 \\ 3 \end{bmatrix}, \quad \phi^2 = \begin{bmatrix} 1 \\ \dfrac{-10+20\gamma}{2+8\gamma} \end{bmatrix} \sim \begin{bmatrix} 1 \\ -3 \end{bmatrix} \tag{2-25}$$

The mode shapes show the effect of mass ratio on behaviour of the system. For small values of γ the TMD must displace approximately 3 times the isolation layer. A higher mass ratio decreases the displacement of the second floor, and when T_2 approaches T_1 the mode shapes are approach $\begin{bmatrix} 1 \\ 1 \end{bmatrix}$ and $\begin{bmatrix} 1 \\ -1 \end{bmatrix}$ reduces the roof displacement of the system. This positive effect of increased mass ratio on the behaviour of TMDs has been shown in other studies (Hoang et al., 2008 and Taniguchi et al., 2008).

2-1-4- Peak Displacements

The modal damping ratios β_n^* are found as

$$2\omega_n^*\beta_n^* = \frac{\phi^{n^T}\boldsymbol{c}\phi^n}{\phi^{n^T}\boldsymbol{m}\phi^n} \quad 2\text{-}26$$

Where $\boldsymbol{c}$ and $\boldsymbol{m}$ are

$$\boldsymbol{m} = \begin{bmatrix} m_1 + m_2 & m_2 \\ m_2 & m_2 \end{bmatrix},\ \boldsymbol{c} = \begin{bmatrix} c_1 & 0 \\ 0 & c_2 \end{bmatrix} \quad 2\text{-}27$$

Identifying L_1, L_2, ω_1^*, ω_2^* and β_1* and β_2*, the maximum modal displacements (q_1 and q_2) can be estimated

$$|q_1|_{max} = L_1 D\ (\omega_1^*, \beta_1^*) \quad 2\text{-}28$$

$$|q_2|_{max} = L_2 D\ (\omega_2^*, \beta_2^*) \quad 2\text{-}29$$

In which D is the displacement from the response spectrum for the appropriate frequency and damping. The complete quadratic combination (CQC) and the square root of the sum of squares (SRSS) are the two presented methods of modal combination that used to determine the peak values of the total responses in modal analysis. The maximum combined story drifts of the first and second DOF (v_{1max} and v_{2max}) can be presented by SRSS method as

$$|v_1|_{max} = [(\phi_1^1|q_1|_{max})^2 + (\phi_1^2|q_2|_{max})^2]^{1/2} \quad 2\text{-}30$$

$$|v_2|_{max} = [(\phi_2^1|q_1|_{max})^2 + (\phi_2^2|q_2|_{max})^2]^{1/2} \quad 2\text{-}31$$

The SRSS method provides an excellent estimate of the peak total response for structures with well-separated natural frequencies, however the CQC rule considers the effect of modal interactions which is more accurate for the cases that the structure's natural frequencies are bound together.

Considering r_0 as the peak value of the total response (Chopra, 1995).

$$r_0 \cong \left(\sum_{n=1}^{N} r_{n0}^2 + \sum_{i=1}^{N}\sum_{n=1}^{N} \rho_{in} r_{i0} r_{n0}\right)^{1/2}, \qquad i \neq n \quad 2\text{-}32$$

In which i and n represent the i^{th} and n^{th} modes, r_{n0} is the peak modal response, N represents the number of modes, and ρ_{in} is the correlation coefficient for the modes. The equation for the correlation coefficient from the work done by Der Kiureghian (1981) is

$$\rho_{in} = \frac{8\sqrt{\beta_i \beta_n}\,(\frac{\omega_i}{\omega_n}\beta_i + \beta_n)(\frac{\omega_i}{\omega_n})^{3/2}}{(1-\beta_{in}^2)^2 + 4\beta_i\beta_n\left(\frac{\omega_i}{\omega_n}\right)\left(1+\left(\frac{\omega_i}{\omega_n}\right)^2\right) + 4(\beta_i^2+\beta_n^2)\left(\frac{\omega_i}{\omega_n}\right)^2} \quad 2\text{-}33$$

The maximum combined story drifts of the first and second DOF (v_{1max} and v_{2max}) can be presented by CQC method as

$$|v_1|_{max} = [(\phi_1^1|q_1|_{max})^2 + (\phi_1^2|q_2|_{max})^2 + \rho_{12}\phi_1^1|q_1|_{max} * \phi_1^2|q_2|_{max} + \rho_{21}\phi_1^1|q_1|_{max} * \phi_1^2|q_2|_{max}]^{1/2} \quad 2\text{-}34$$

$$|v_2|_{max} = [(\phi_2^1|q_1|_{max})^2 + (\phi_2^2|q_2|_{max})^2 + \rho_{12}\phi_2^1|q_1|_{max} * \phi_2^2|q_2|_{max} + \rho_{21}\phi_2^1|q_1|_{max} * \phi_2^2|q_2|_{max}]^{1/2} \quad 2\text{-}35$$

As an example the peak displacements from SRSS and CQC methods are shown in Fig. 2-4 for a dual isolation model with $\gamma = 0.5$, $\beta_1 = 0.15$, $\beta_2 = 0.15$ and $T_1 = 3.5$ s, when the period of the second DOF varies from 0.3 T_1 to 2 T_1.

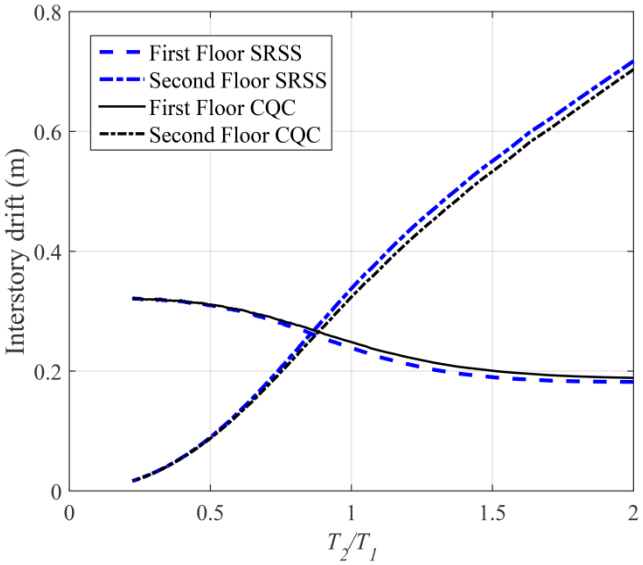

Figure 2-4: Comparing CQC and SRSS methods, T_1= 3.5 s, γ = 0.5, $\beta_1 = \beta_2 = 0.15$

Because the floor displacements from the SRSS method are in good agreement with results from CQC over a wide range of mass and frequency ratios, SRSS is used as modal combination method in this study.

2-2- Modal Response Spectrum Analysis

In order to validate the analytically derived equations, a set of analyses have been conducted on the 2DOF model shown in Fig. 2-2, when the mass ratio γ of the dual isolation system was chosen as 0.5, locating the second isolation layer at mid height of the building. The period of the first isolation layer T_1, was chosen as 3.5 s and the damping ratio of the first and second layers (β_1 and β_2) were chosen as 15%. This dual isolation system was then analysed using response spectrum analysis for a design basis earthquake (DBE), the spectrum for which is shown in Fig. 2-5. The spectrum is defined for 10% probability of exceedance in 50 years downtown Seattle, WA, USA (47.60,-122.34) and soil type D (ASCE 07, 2010). The analytical results from binominal expansion of the equation of motions are compared to the numerical solutions. Figure 2-6 shows the comparison between numerical and analytical natural frequencies, derived from Eq. 2-11 and 2-16 for Case 1 and Case2. Figure 2-7 shows the story drifts from the analytical and numerical solutions. It can be seen that the analytically derived solutions are valid over a wide range of period combinations.

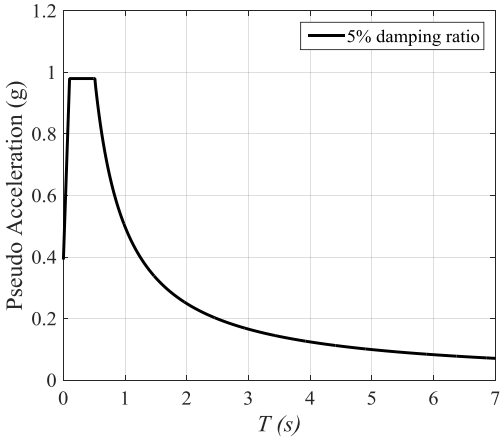

Figure 2-5: Design Spectrum, Soil type D, Damping ratio 5%

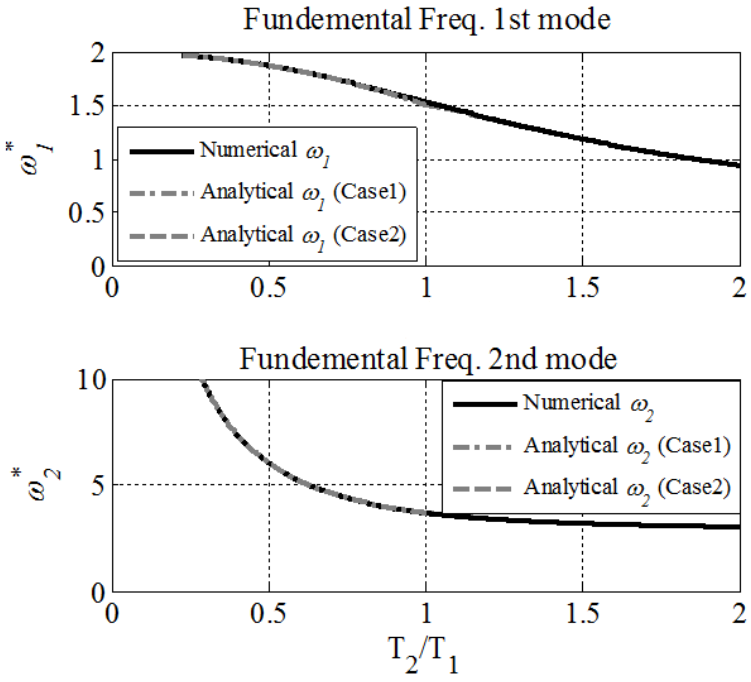

Figure 2-6: Comparing the numerical and analytical natural frequencies, T_1 = 3.5 s, γ = 0.5, β_1 = 0.15, β_2 = 0.15

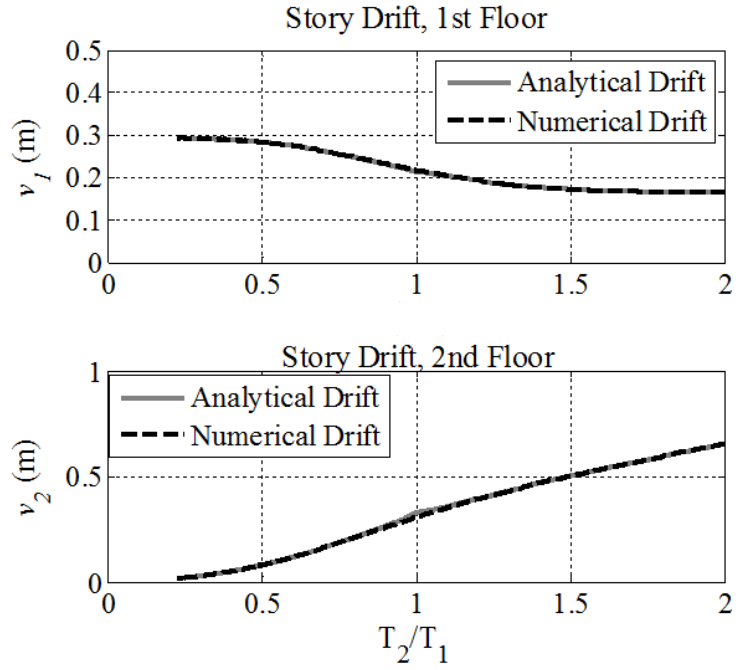

Figure 2-7: Comparing the numerical and analytical story drifts (SRSS) T_1 = 3.5 s, γ = 0.5, β_1 = 0.15, β_2 = 0.15

The analytical method developed in this chapter to estimate the modal parameters of the two DOF model creates the foundation to assess the behaviour of various types of anti-seismic systems such as classic isolation, tuned mass damper, mid-story isolation and dual isolation and to identify the parameters that has an impact on the behaviour of these systems. These effective parameters will be discussed in Chapter 3 to optimize the behavior of dual isolation system.

3- Tuning of System Parameters

3-1- Behaviour of Dual Isolation System

From the examination of the theoretical results of mid-story isolation and base isolation with TMD, it is seen that the displacement demands on the second DOF decrease with larger values of γ and increase with larger T_2, while the increase in T_2 reduces the displacement demand of the first DOF. These insights are used to select the preliminary parameters for the proposed dual isolation system. The same two DOF model shown in Fig. 2-2 is used for a numerical response spectrum study. As a starting point the mass ratio γ of the dual isolation system is chosen as 0.5, locating the second isolation layer at the mid height of the building, and the period of the first isolation layer T_1, is chosen as 3.5 s. The damping ratio of the first and second DOFs, β_1 and β_2 were chosen as 15%, this is a typical level of damping for isolation and is significantly larger than seen in TMD systems for which the damping is roughly 5%. Depending on the type of isolation bearing selected as well as any addition viscous or hysteretic dampers, isolation layers typically exhibit damping in the range of 10-35%.

This dual isolation system was then analyzed using response spectrum analysis for a design basis earthquake (DBE), the spectrum for which is shown in Fig. 2-5. The maximum relative displacements of each DOF are presented in Fig. 3-1, varying the period of the second isolation layer, T_2. The left side of the graph represents the traditional base isolation system in which the natural period of the first DOF is much longer than the second DOF. As the period of the second DOF increases, the drift of the first DOF is reduced with the concession of increased drifts in the second DOF. This finding is in line with the theory explored in the previous section.

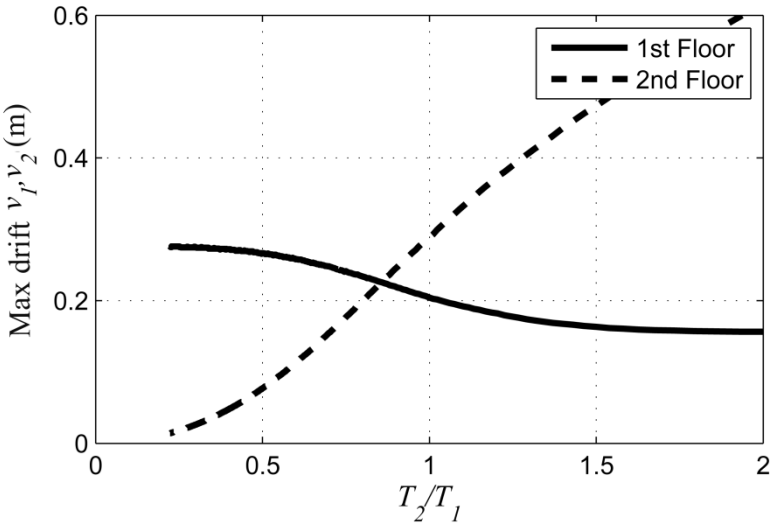

Figure 3-1: Story drifts found using response spectrum analysis, T_1 = 3.5 s, $\beta_1 = \beta_2 = 0.15$

Compared to the classic base isolation system, the participation factor of the first mode is decreased, reducing the first DOF's displacement. For the case when T_2 approaches T_1 the modal participation factor is equal to 0.5 for both the first and second modes. Although selecting a larger period range for the new system leads to further reduction in drifts of the first isolation layer, it generates large demands for the second isolation layer.

Unlike in TMD systems, in which only the displacement of the first DOF must be accommodated, both displacement DOFs will need to be accommodated for dual isolation. As the absolute displacement at the second DOF is of concern, the middle section of the graph where the period of the second isolation layer approaches the natural period of the first ($T_2/T_1 \rightarrow 1$) is chosen for the new proposed dual isolation system.

The effect of the mass ratio γ and damping ratios β_1 and β_2 are studied in order to find an optimal state for the system to have the same effect but with less displacement of the second DOF. The result of the response spectrum analysis is presented in Fig. 3-2 for a model with T_1 = 3.5 s and $\beta_1 = \beta_2 = 0.15$. The mass ratio is altered from 0.1 to 0.9 while keeping the first floor's period at a constant value. The increase in γ reduces the increase in the second isolation layer's displacement, as shown in Fig. 3-2, and therefore reduces

the overall roof displacement. Thus, increasing the mass of the second DOF improves the behaviour of the dual isolation system.

The effect of β_1 is presented in Figure 3-3 (a) in which $\beta_2 = 0.15$ is kept constant while β_1 is varied from 0.1 to 0.2. As β_1 increases, the maximum displacements of the first and second DOFs decrease, however it does not increase the efficiency of the system in reducing the lateral displacement of the first isolation layer and roof displacement compared to classic isolation model. For example, when β_1 is 10%, the dual isolation system reduces the first floor displacement by 30% from classic base isolation; however, when β_1 is 20% the reduction is only 18%. Thus, low to moderate damping values for the first DOF are recommended.

Figure 3-3 (b) shows the effect of β_2 on the floor's displacement, with $\beta_1 = 0.15$ constant while β_2 varies from 0.1 to 0.35. Damping in the second isolation layer is shown to have significantly higher effect; larger β_2 decreases the displacements of both the first and second DOF. Based off of these results, β_2 is suggested as 35% for the system.

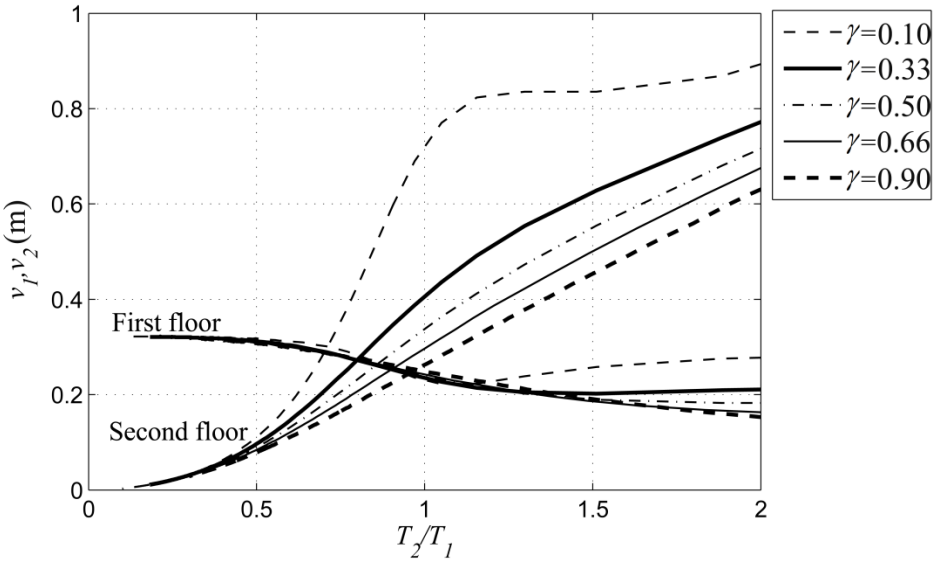

Figure 3-2: Effect of mass ratio on the displacements of the dual isolation system T_1 = 3.5 s, β_1 = β_2 = 0.15

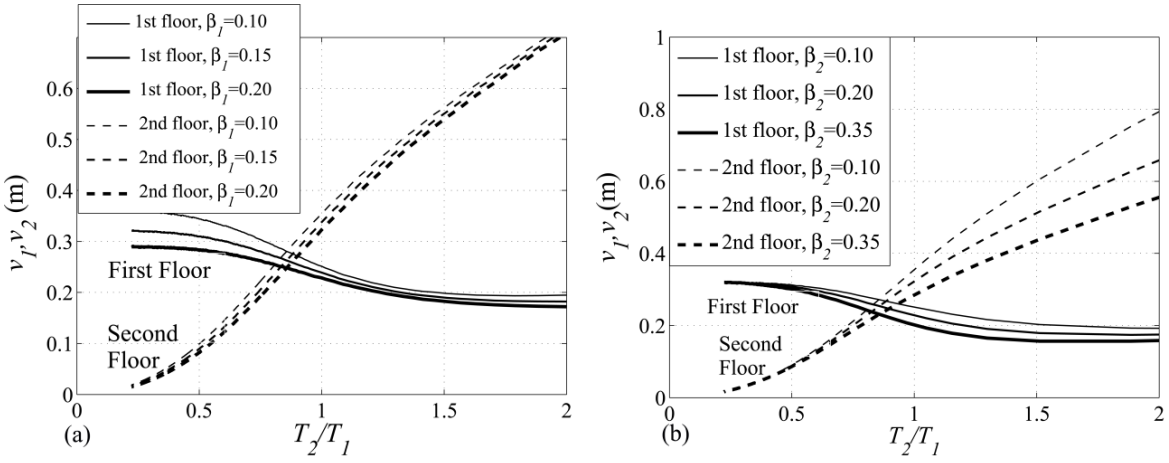

Figure 3-3: (a) Effect of β_1 while β_2 = 0.15, (b) effect of β_2, while β_1 = 0.15 on the displacements of the dual isolation system, T_1 = 3.5 s.

3-2- Conceptual Design

As shown in Fig. 3-2, the dual isolation system is effective in reducing the displacement demand of the structure below the second isolation layer, the total roof displacement from adding the interstory drifts of the first and second floors can be roughly similar to the displacement that occurs at classic base isolation models. Two conceptual designs for the potential practical application of the dual isolation system are presented in this section. Both designs will result in an increased number of bearings as compared to classical isolation, but bearing sizes may be reduced by up to half. Both designs will increase the costs due to architectural and mechanical detailing necessary for the isolation layers. However, as the system offers large decreases in acceleration demands for the upper portion of the building, these extra costs may be warranted for some applications.

3-2-1- Inner Story Separation

Inner story separation, shown in Fig. 3-4 and Fig. 3-5, is one of the proposed design schemes that reduces the displacement of the first DOF and simultaneously limits the movement of the above superstructure so that the total displacement of the structure does not exceed the first layer. The bearings are installed under the columns of the first floor

and the upper floor's inner columns. Figure 3-4, and Figure 3-5 show the floor plan and the section view A-A of the proposed system respectively.

A similar design has been implemented by Kidokora (2008) in which the floor masses were used as a large tuned mass damper for a fixed base structure. In this configuration the total displacement of the building is governed by the reduced displacement for the first isolation layer, however the available floor space for all floors above the second isolation are decreased.

3-2-2- Floor Separation

The second design divides the total displacement of the isolation layer between two layers as shown in Figure 3-6. This design will decrease the lateral displacement of the building up to a certain height. This method may be suitable for taller buildings in the vicinity of shorter structures when the goal is to limit the base displacement and to distribute the residual lateral drift above the height of the adjacent building.

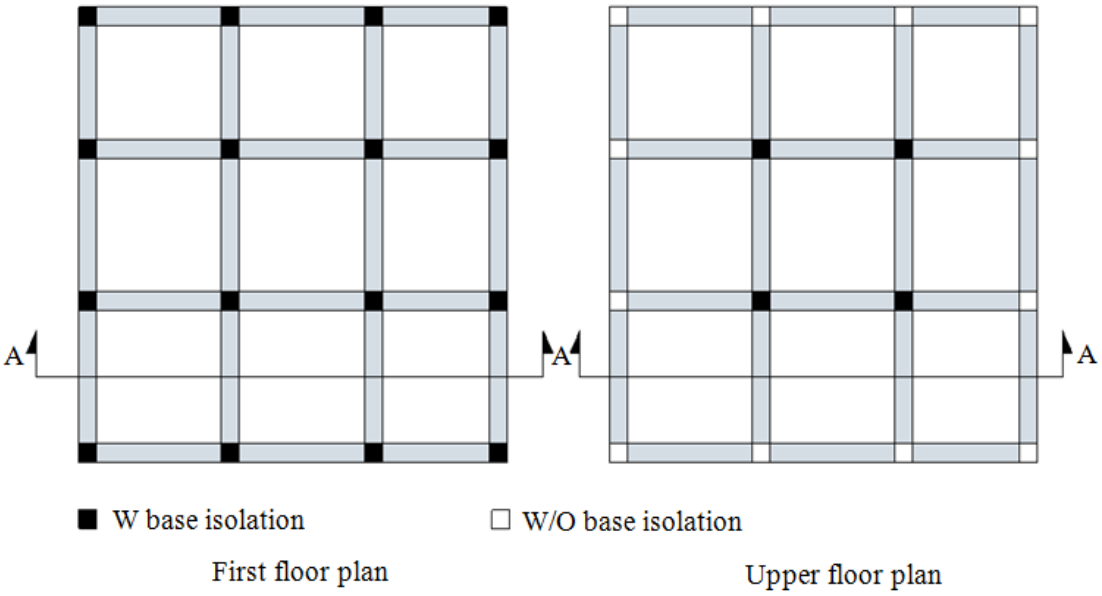

Figure 3-4: Floor plan, inner story separation

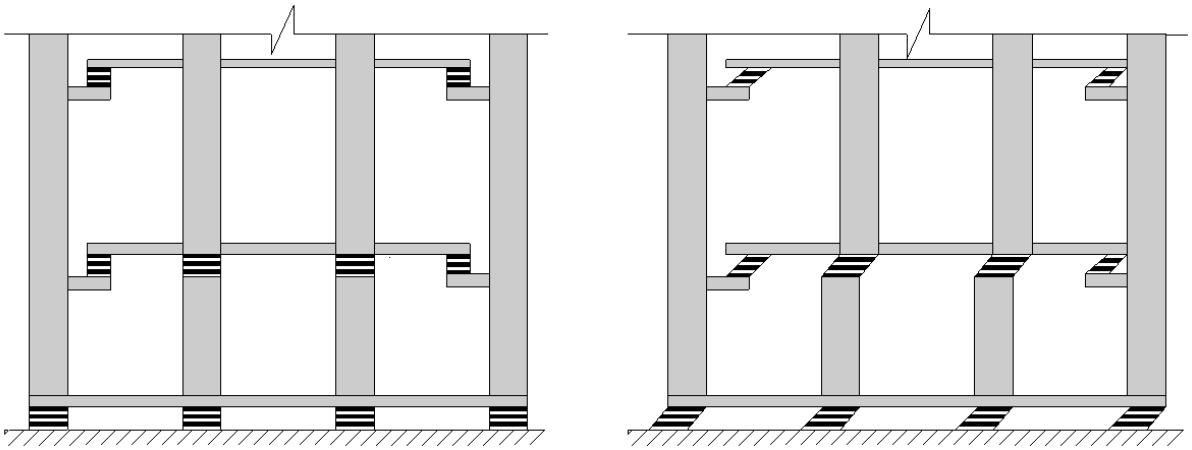

Figure 3-5: Section view A-A, inner story separation

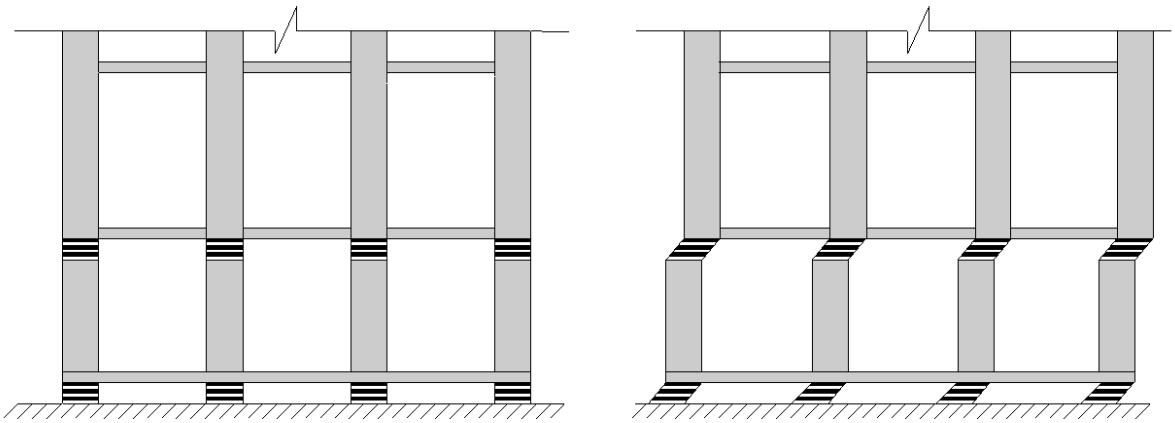

Figure 3-6: Story separation

3-2- Sensitivity to Soil Conditions

To examine the robustness of the dual isolation system in varying soil conditions and its effectiveness compared to conventional isolation as well as base isolation with tuned mass damper (BI-TMD) in reducing the displacement of an isolated structure, the response of the structure to a stationary stochastic excitation with a power spectral density proposed by Kanai (1957) and Tajimi (1960) is investigated. The mean square of the structure's displacement is given by

$$J = \int_{-\infty}^{+\infty} |H(\omega)|^2 s(\omega) d\omega \tag{3-1}$$

in which $H(w)$ is the complex frequency response of the system and $s(\omega)$ is the power spectral density (PSD) of the ground motion. When the performance index J is minimized, the system exhibits efficient performance. The complex frequency response function for a 2DOF model can be analytically obtained by substituting (Crandall & Mark, 1963).

$$\ddot{u}_{g0} = e^{i\omega t}, \begin{cases} H_{v1}(\omega) e^{i\omega t} & \text{for } v_1 \\ H_{v2}(\omega) e^{i\omega t} & \text{for } v_2 \end{cases} \tag{3-2}$$

in equation of motion (Equations 2-4 and 2-5). Therefore the transfer function for each relative DOF is

$$H_{v_1}(\omega) = \frac{\left(1 - \frac{m_2}{M}\right)\omega^2 - \frac{c_2}{m_2} i\omega - \frac{k_2}{m_2}}{\left(-\omega^2 + \frac{c_2}{m_2} i\omega + \frac{k_2}{m_2}\right)\left(-\omega^2 + \frac{c_1}{M} i\omega + \frac{k_1}{M}\right) - \frac{m_2}{M}\omega^4} \tag{3-3}$$

$$H_{v_2}(\omega) = \frac{-1 + \omega^2 H_{v_1}(\omega)}{\left(-\omega^2 + \frac{c_2}{m_2} i\omega + \frac{k_2}{m_2}\right)} \tag{3-4}$$

the PSD of the ground motion is denoted by

$$s(\omega) = \frac{\omega_g^4 + 4\xi_g^2 \omega_g^2 \omega^2}{(\omega_g^2 - \omega^2)^2 + 4{\xi_g}^2 \omega_g^2 \omega^2} \; G_0 \tag{3-5}$$

where ω_g, G_0 and ξ_g are the characteristic ground frequency, white noise intensity and damping ratio, respectively. For this study the parameters of Kanai-Tajimi model ω_g and ξ_g are selected as specified in Table 1 for soft, medium and stiff soil conditions based on work by Der Kiureghian, (1996).

To investigate the robustness of system and the effect of second isolation layer in reducing the displacement demand of the first isolation layer the response ratio J_1/J_0 and J_2/J_1 is investigated in which J_0 represents the mean square of the displacement response of the classic base isolated structure with T = 3.5 s and β = 0.15. J_1 and J_2 are the mean

square of the displacement response of the first and second DOF in dual isolation system. The normalized expected response of the system J_1/J_0 and J_2/J_1 are independent of G_0. The effectiveness of the hybrid base isolation-tuned mass damper system (BI–TMD) with T_1 = 3.5 s, β_1 = 0.15 and mass ratio γ = 0.05 is shown in Figure 3-7 for stiff soil conditions. The selected mass ratio is within the range of 0.01 to 0.10 which was used for TMD systems in the study done by Taniguchi et al. (2008). It can be seen that the tuned mass damper is most effective in reducing the response in a limited range, roughly $1 < T_2/T_1 < 1.5$. Figure 3-8 shows the ratio of the performance index for the dual isolation system ($\gamma = 0.9$) for stiff and soft soil conditions. Compared to the BI-TMD system, the dual isolation system is more effective in reducing the response for larger range of frequency ratios. It is shown that for the dual isolation system with this specific design (γ = 0.9, β_1 = 0.15 and T_2/T_1 = 1), increasing β_2 is effective until reaching

Table 1: Kanai - Tajimi parameters for different soil types (Der Kiureghian, 1996)

Soil Type	ω_g	ξ_g
Stiff	6π	0.6
Medium	3π	0.4
Soft	π	0.2

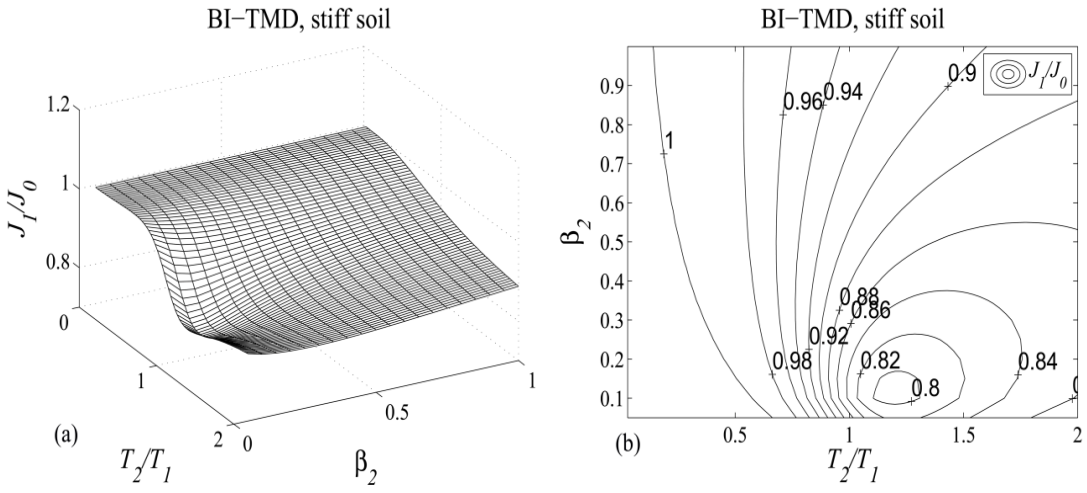

Figure 3-7: Effect of TMD on base isolated system (a) Normalized mean square response of first DOF displacement in stiff soil, (b) contour plot of (a)

a value between 30% and 40%, after which reductions in displacements are minimal. Table 2 shows displacement reductions for a specific case in which $T_1 = T_2$ and $\beta_2 = 0.35$ to compare different soil types. The system works well for all the soil types. Interestingly, the results indicate that the dual isolation system is more effective for reducing first floor displacements in softer soil.

Table 2 : Effect of soil type on systems response, $T_1 = T_2 = 3.5$ s, $\beta_1 = 0.15$, $\beta_2 = 0.35$

System	Soil type	J_1/J_0	J_2/J_1
Base isolation w TMD	Stiff	0.85	1.79
Dual isolation	Stiff	0.61	0.90
Dual isolation	Medium	0.60	0.90
Dual isolation	Soft	0.43	0.90

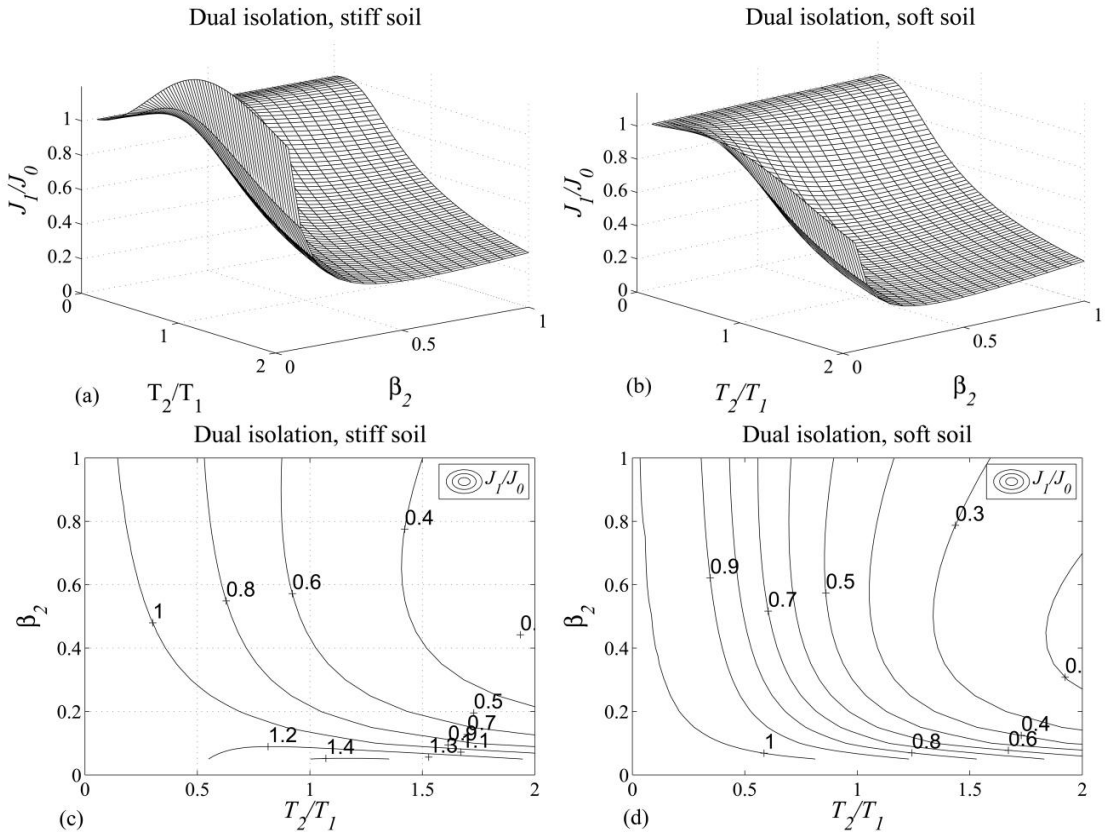

Figure 3-8: Normalized mean square response of the first DOF displacement. (a) Effectiveness of dual isolation in stiff soil, (b) effectiveness of dual isolation in soft soil, (c) contour plot for stiff soil, (d) contour plot for soft soil

Figure 3-9 shows the amplification in the displacement of the second isolation layer in dual isolation system and in the TMD layer in BI-TMD system. As shown, the increased mass of the dual isolation system helps to reduce the large amplification at the second DOF. At $T_2/T_1 = 1$ and $\beta_2 = 0.35$, the response of the TMD is roughly two times greater than the second isolation layer with larger mass ratio. These findings are as expected from the response spectra analysis presented earlier. In case of non-stationary excitations, i.e. earthquake ground motions, there will be significant variation in displacement demands of the first and second DOFs.

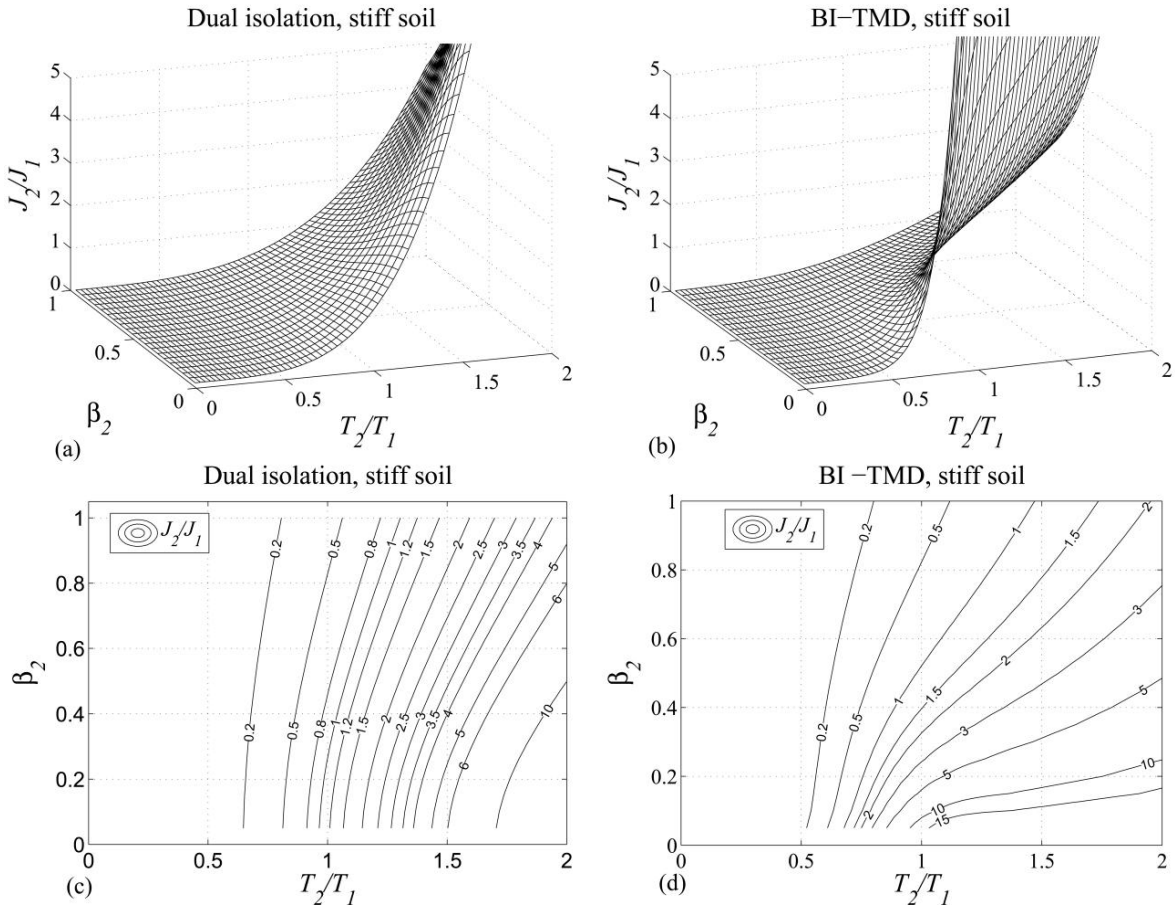

Figure 3-9: (a) Effectiveness of dual isolation in stiff soil (J_2/J_1), (b) effectiveness of BI-TMD in stiff soil, (c) contour plot for stiff soil, (d) contour plot for BI-TMD, $T_1 = T_2 = 3.5$s, $\beta_1 = 0.1$

4- Time History Analysis

To evaluate the performance of the dual isolation system compared to classic base isolation, a suite of ten ground motions, including five pulse motions, scaled to the DBE spectrum (Fig 2-5) was selected. The ground motion specifications are listed in Table 3. The response spectra of the ground motions are shown in Figure 4-2. Only the fault normal components of the ground motions were used.

4-1- Linear Systems

From the response spectrum analysis, the ratio of the frequencies of the two isolation systems was selected to be one, and a larger mass ratio γ was found to improve the efficiency of the system in minimizing the displacements of both degrees of freedom, so a mass ratio of 0.9 was selected. In addition, a low to moderate damping ratio for the first isolation layer and a larger damping ratio for the second isolation layer were found to improve the behavior of the system. Following the response spectrum analysis, a ten story building (Fig. 4-1) with two isolation layers at the base and second floor, with a mass ratio γ = 0.9, a moderate damping ratio β_1 = 0.15, for the first isolation layer, and a high damping ratio β_2 = 0.35, for the second isolation layer is selected for the linear time history analysis.

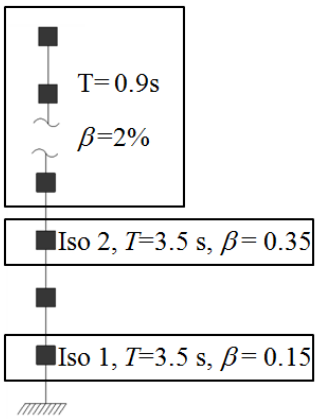

Figure 4-1: 10 story dual isolation model

Table 3: Selected ground motions

#	NGA Record #	Earthquake	Year	Station	Scale Factor	Pulse Period
1	778	Loma Prieta	1989	Hollister Diff. Array	1.624	-
2	1158	Kocaeli	1999	Duzce	0.855	-
3	1203	Chi Chi	1999	CHY036	1.35	-
4	1633	Manjil	1990	Abbar	1.475	-
5	5829	El Mayor	2010	RITTO	1.223	-
6	181	Imperial Valley	1979	El Centro Array #6	1.024	2.6
7	316	Westmorland	1981	Parachute Test Site	1.84	3.6
8	721	Superstition Hills	1987	El Centro Emp. Co	1.588	2.4
9	143	Tabas	1978	Tabas	0.584	6.18

The dual isolation system considered for this analysis has a nominal period of 3.5 s for both isolation layers. The period of the single-story superstructure on top of the first isolation layer is 0.25 s, and the period of the nine-story superstructure on the second isolation layer is T_s=0.9 s. Both superstructures are assigned 2% Rayleigh damping and they are assumed to have completely linear elastic behaviour.

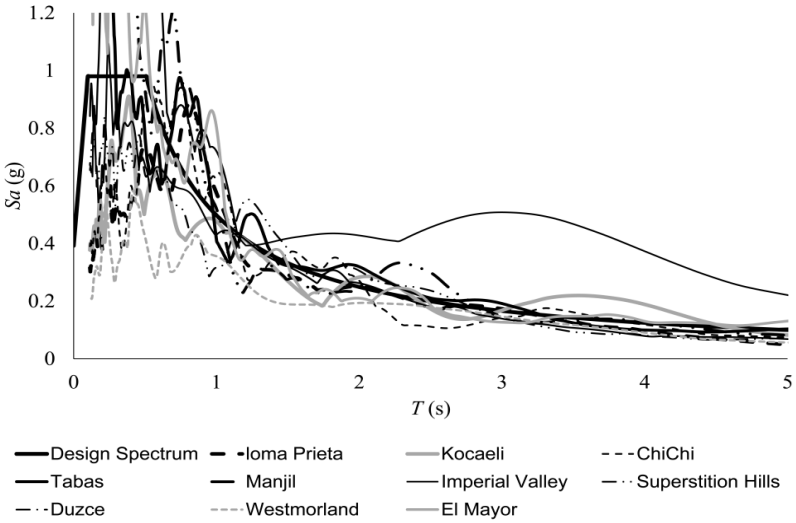

Figure 4-2: Ground motions response spectrum

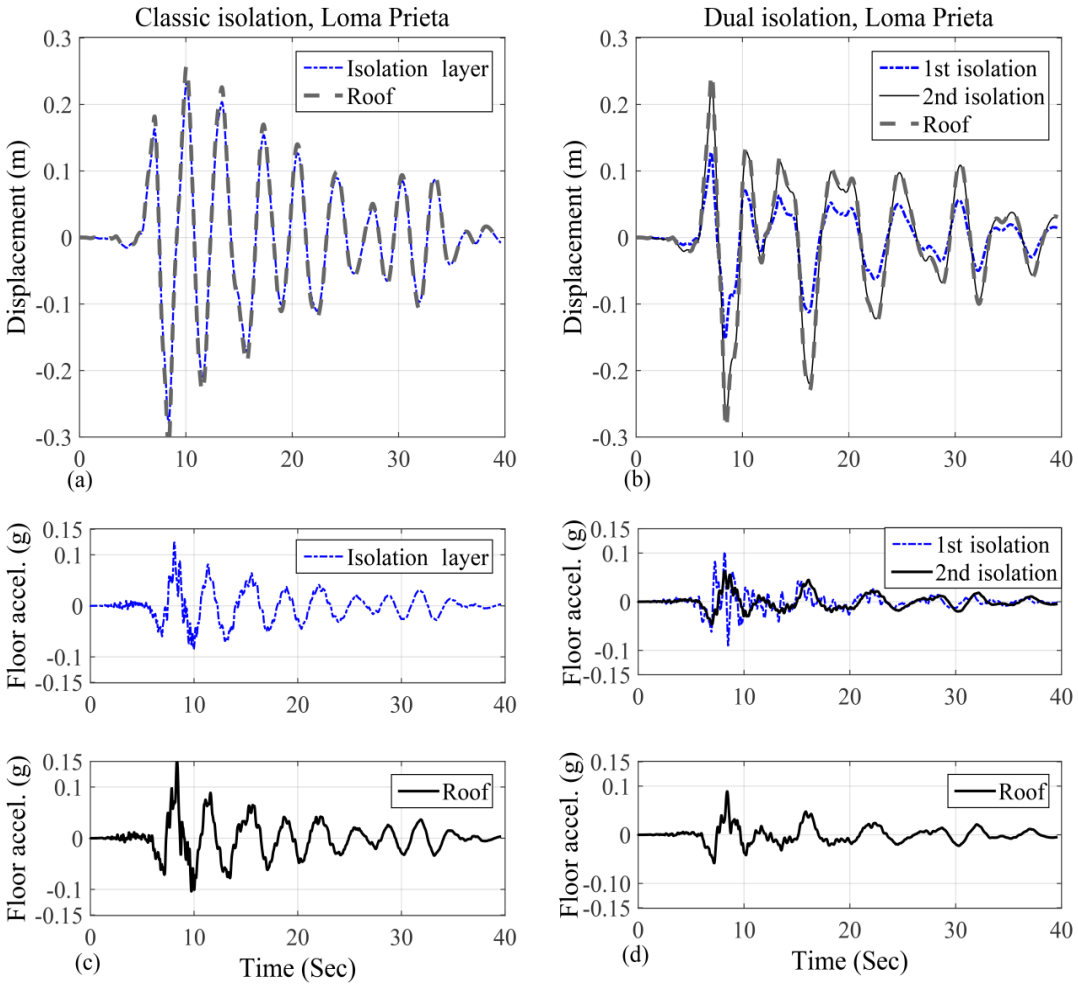

Figure 4-3: Time history analysis, Loma Prieta, (a) classic isolation, displacement, (b) dual isolation displacement, (c) classic isolation acceleration, (d) dual isolation acceleration. dual isolation: $T_1 = T_2 = 3.5$ s, $\beta_1 = 0.15$, $\beta_2 = 0.35$, $T_s = 0.9$ s, classic isolation: $T_1 = 3.5$ s, $\beta_1 = 0.15$, $T_s = 1$s

For comparison, the classic base isolated system consists of an isolation layer ($T = 3.5$ s, $\beta = 0.15$) at the base with a ten story superstructure with the fundamental period $T_s = 1$ s with 2% Rayleigh damping. The peak displacement and floor acceleration responses to seismic excitations for all motions are listed in Table 4 and Table 5 respectively. The analysis was run using Newmark's time-stepping method for linear systems in MATLAB. The time history of the floor absolute displacement and acceleration responses of the dual isolation and classic isolation are presented in Fig. 4-3 to Fig. 4-6 for Loma Prieta, El Mayor, Imperial Valley and Duzce motions.

Table 4: Peak response displacements to seismic excitation

Ground motion	Classic Base Isolation		Dual Isolation		
	u_1 (m)	u_{10} (m)	u_1 (m)	u_2(m)	u_{10} (m)
Loma Prieta	0.28	0.31	0.15	0.28	0.29
Kocaeli	0.42	0.46	0.22	0.44	0.46
Chi Chi	0.24	0.27	0.17	0.32	0.34
Manjil	0.32	0.36	0.18	0.35	0.37
El Mayor	0.28	0.31	0.26	0.49	0.52
Imperial Valley	0.95	1.06	0.56	1.08	1.14
Westmorland	0.25	0.27	0.12	0.23	0.24
Superstition Hills	0.22	0.25	0.12	0.24	0.25
Tabas	0.29	0.32	0.19	0.36	0.38
Duzce	0.21	0.23	0.14	0.27	0.28

Table 5: Peak response acceleration to seismic excitation

Ground motion	Classic Base Isolation		Dual Isolation		
	A_1 (g)	A_{10} (g)	A_1 (g)	A_2 (g)	A_{10} (g)
Loma Prieta	0.12	0.15	0.10	0.06	0.09
Kocaeli	0.14	0.15	0.12	0.08	0.08
Chi Chi	0.09	0.10	0.11	0.06	0.07
Manjil	0.17	0.19	0.17	0.09	0.10
El Mayor	0.16	0.18	0.11	0.10	0.11
Imperial Valley	0.33	0.37	0.19	0.21	0.22
Westmorland	0.08	0.09	0.07	0.05	0.06
Superstition Hills	0.10	0.10	0.12	0.08	0.07
Tabas	0.16	0.17	0.12	0.10	0.11
Duzce	0.20	0.20	0.17	0.07	0.08

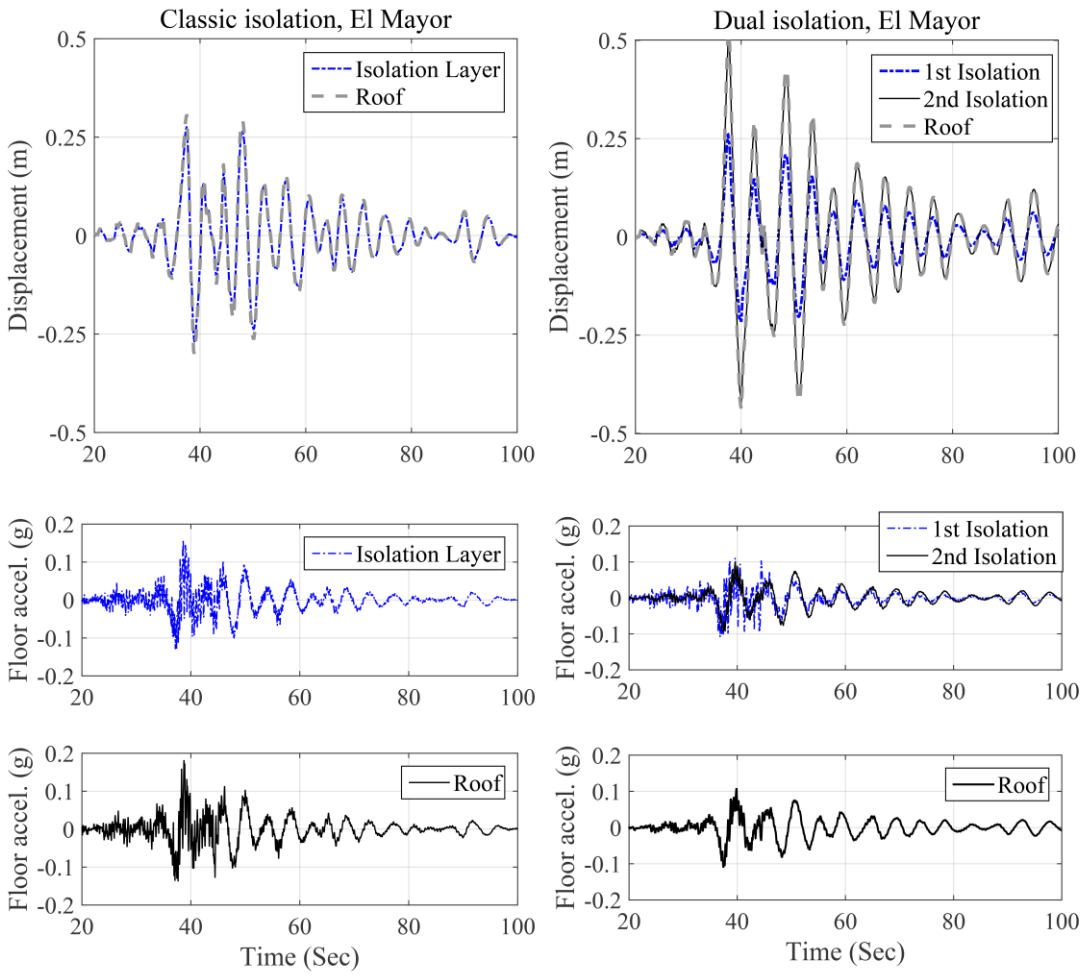

Figure 4-4: Time history analysis, El Mayor, (a) classic isolation, displacement, (b) dual isolation displacement, (c) classic isolation acceleration, (d) dual isolation acceleration. Dual isolation: T_1 = T_2 = 3.5 s, β_1 = 0.15, β_2 = 0.35, T_s = 0.9 s, classic isolation: T_1 = 3.5 s, β_1 = 0.15, T_s = 1s

With the exception of El Mayor, the relative displacement of the first DOF of the dual isolation system v_1, is reduced significantly for all pulse and non-pulse type motions compared to the classic base isolation system, by up to 50%. However, the total displacement of the second isolation layer u_2, and the total displacement of the roof $u_{10,}$ are increased by 18% and 13% on average compared to the classic isolation system. The efficiency of the dual isolation system depends on the frequency content of the ground motion. Fig. 4-7 shows the frequency content of Loma Prieta, El Mayor, Imperial Valley and Duzce through Fourier amplitude spectra representation.

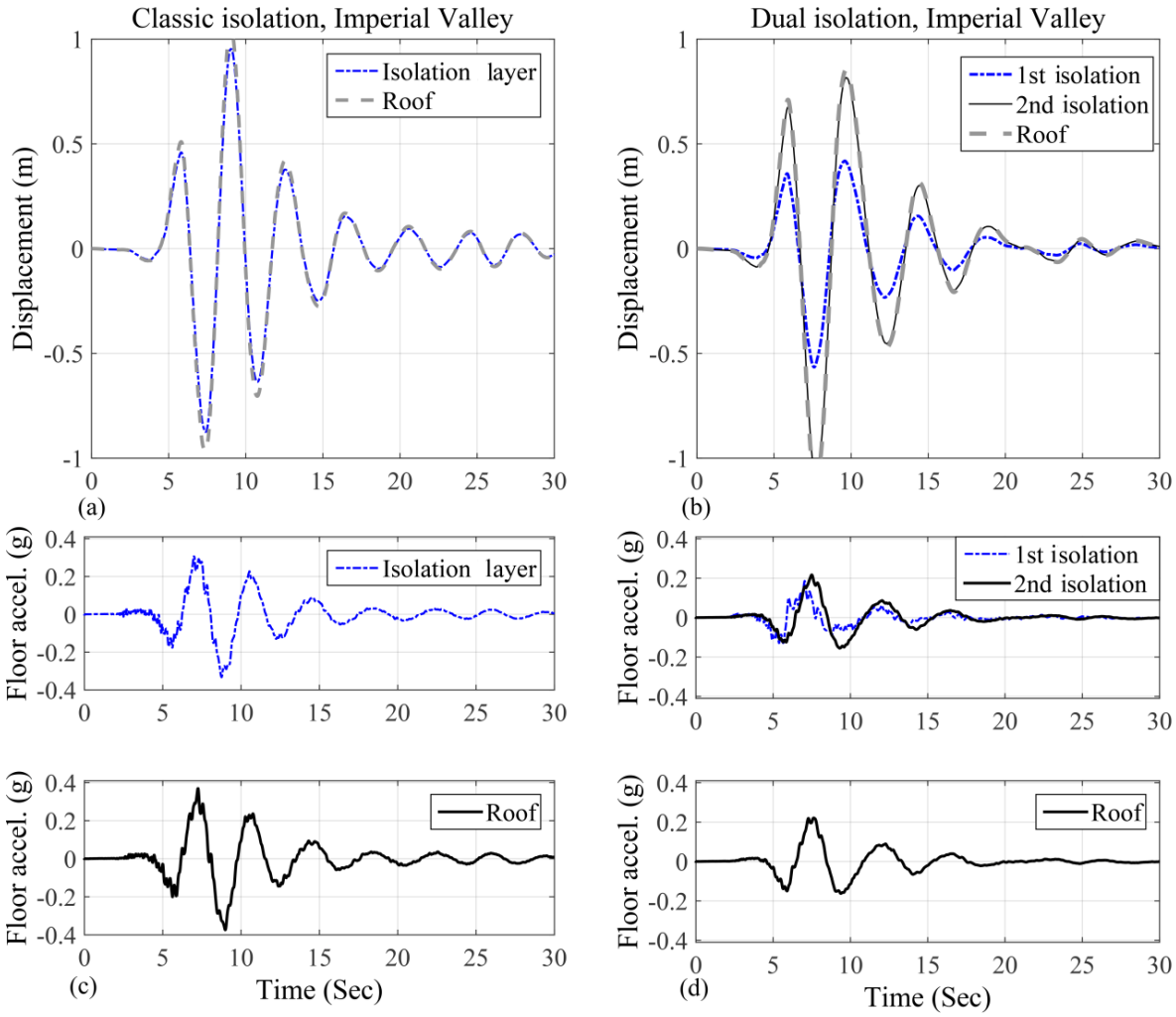

Figure 4-5: Time history analysis, Imperial Valley, (a) classic isolation, displacement, (b) dual isolation displacement, (c) classic isolation acceleration, (d) dual isolation acceleration. Dual isolation: $T_1 = T_2 = 3.5$ s, $\beta_1 = 0.15$, $\beta_2 = 0.35$, $T_s = 0.9$ s, classic isolation: $T_1 = 3.5$ s, $\beta_1 = 0.15$, $T_s = 1$s

The dual isolation system is more effective for motions such as Loma Prieta and Imperial Valley which have more energy in the lower frequency range, between 0.3 to 1 Hz, close to the frequency of the isolated system. For example, the total displacement at second isolation layer, increased by 18% on average, but the increase is negligible for motions with lower frequency content. The dual isolation system is not as effective in reducing the displacement of the first layer for motions such as El Mayor, Duzce and Chi Chi which have high frequency content.

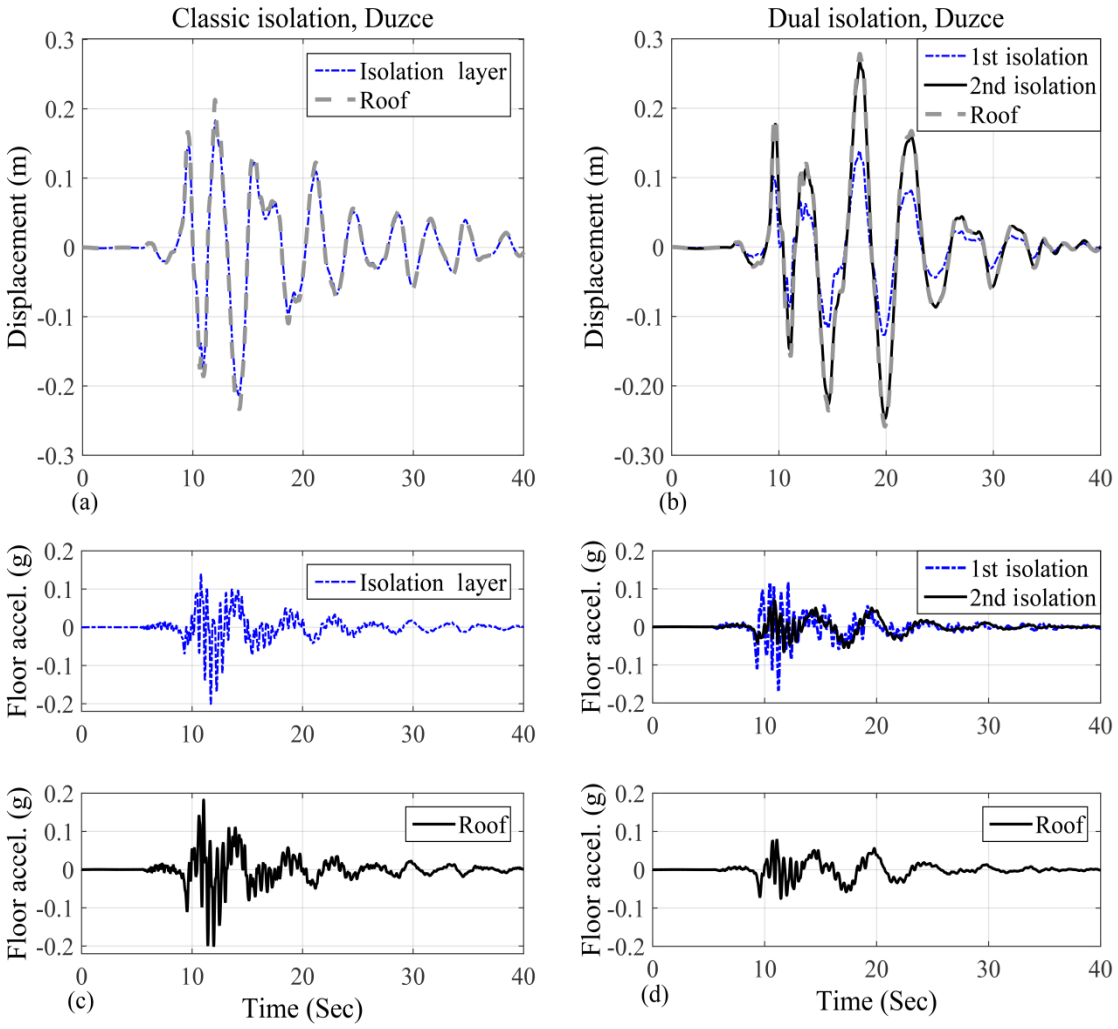

Figure 4-6: Time history analysis, Duzce, (a) classic isolation, displacement, (b) dual isolation displacement, (c) classic isolation acceleration, (d) dual isolation acceleration. Dual isolation: T_1 = T_2 = 3.5 s, β_1 = 0.15, β_2 = 0.35, T_s = 0.9 s, classic isolation: T_1 = 3.5 s, β_1 = 0.15, T_s = 1s.

In the dual isolation system, the peak acceleration of the first DOF is on the same order as those from the classic isolation system. The peak acceleration of the second isolation layer is decreases by 40% on average for all motions. Therefore, a significant reduction in acceleration has been achieved for the majority of the building while the displacement of the first floor has been decreased. This reduction in peak acceleration of the second superstructure increases the protection of acceleration sensitive equipment and nonstructural components and provides occupants with increased comfort.

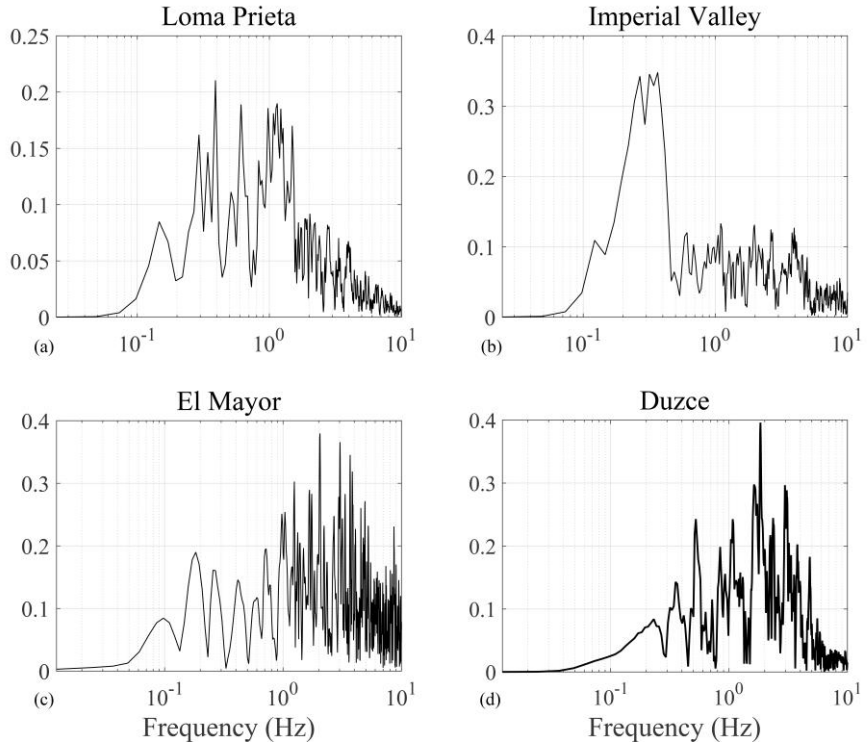

Figure 4-7: Fourier amplitude spectra, (a) Loma Prieta, (b) El Mayor, (c) Imperial Valley, (d) Duzce

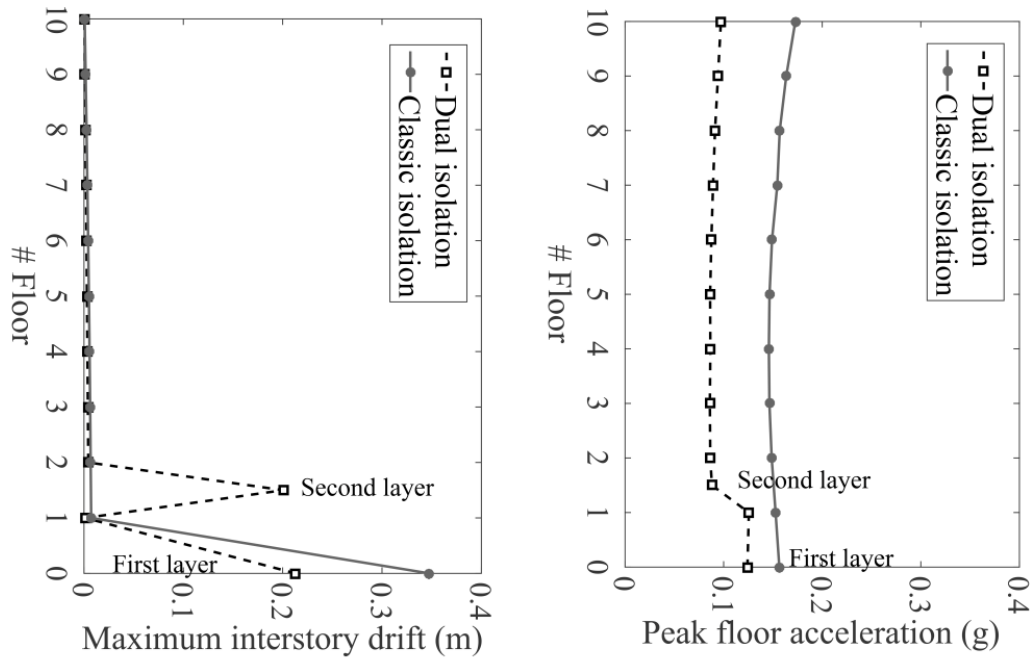

Figure 4-8: Maximum interstory drifts and peak floor accelerations, average of 10 motions

The maximum interstory drifts and the peak floor accelerations, averaged out over 10 ground motions listed in Table 1 are shown in Fig. 4-8 over the height of the building. Moreover, the interstory drifts of selected stories for the Loma Prieta and El Mayor motions are shown for the dual isolation and the classic isolation systems for the significant duration of the motions in Fig. 4-9. In the dual isolation system, the interstory drifts in the superstructure are slightly decreased under the El Mayor motion; however, significantly larger reductions are seen under the lower-frequency Loma Prieta motion.

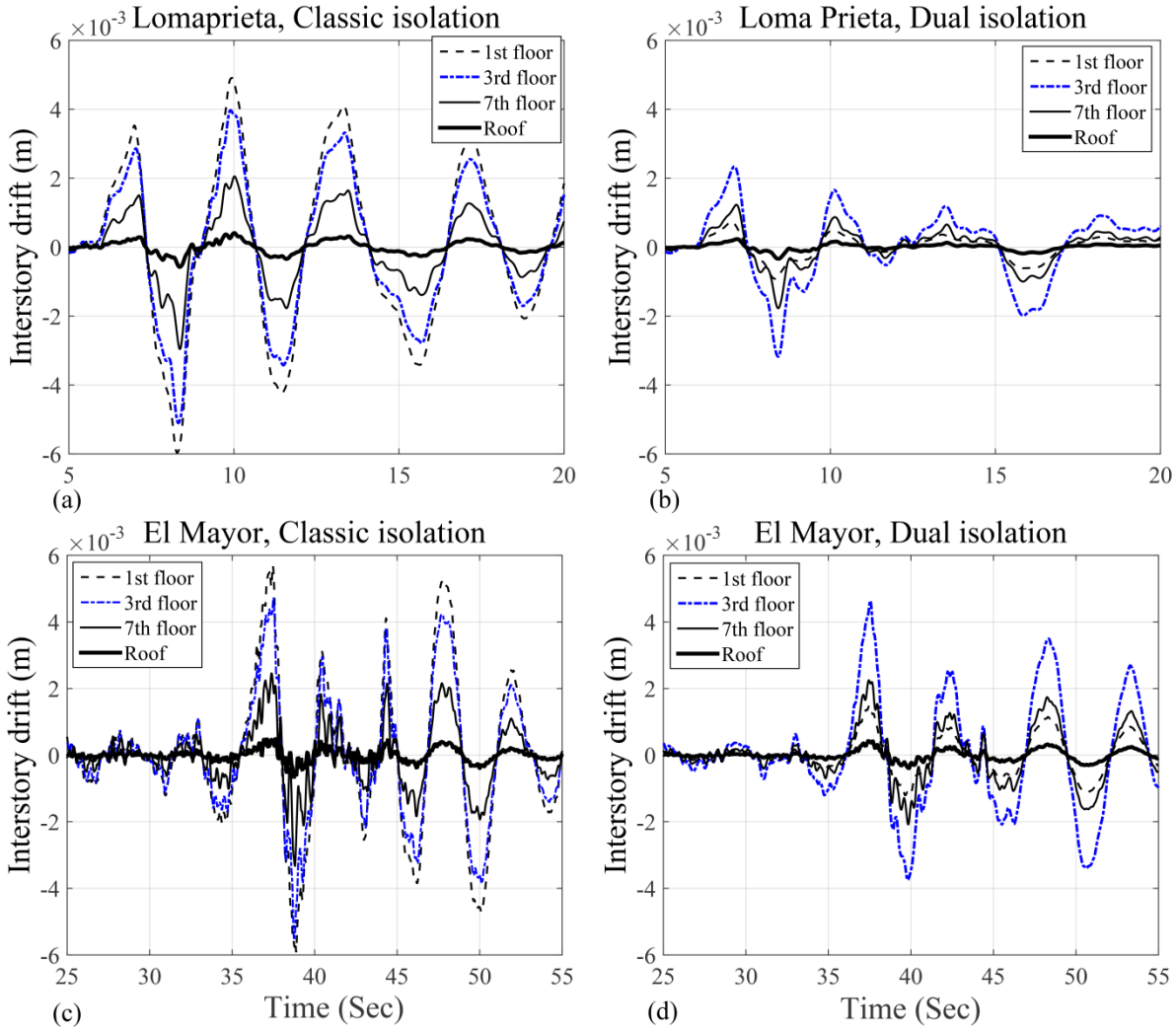

Figure 4-9: Interstory drift time histories at the superstructure, (a) classic isolation, Loma Prieta, (b) dual isolation, Loma Prieta, (c) classic isolation, El mayor, (D) dual isolation, El Mayor

Floor response spectra reflect the effectiveness of the proposed isolation system in protecting building systems and contents in any specific floor of a building. Nonstructural components and building contents are associated with more than 75% of the construction costs (Reinoso and Miranda, 2005) and have a direct role in maintaining the operation of the building after ground motions. Suspended ceilings, heating-ventilation and air conditioning (HVAC) systems and elevators are example of non-structural acceleration sensitive systems. Examples of acceleration sensitive contents include file cabinets, computer systems, book shelves, and power generation systems.

The response spectra of the classic and dual isolation systems are shown in Fig. 4-10, for Loma Prieta, El Mayor, Imperial Valley and Duzce ground motions. For all motions the demands on contents and systems are significantly reduced in the upper portion of the structure above the second isolation layer in the whole frequency bandwidth. However, for the first floor, the demands are increased significantly in the 1 s period range, close to the second period of the dual isolated structure. While the demands are increased for the first floor, this represents only $1/10^{th}$ of the building floors and thus, a major decrease in demand is seen for the majority of the structural contents.

4-1-1- Base Shear and Overturning Moment

Classic base isolated structures have significantly smaller base shear compared to fixed base structures, However, overturning moments can still cause design issues due to significant tensile loads on isolation bearings, the majority of which cannot sustain large, if any, tensile forces. Table 6 and Fig. 4-11 illustrate the maximum base shears (normalized to total weight of the models) and overturning forces for the dual isolation and the classic isolation systems. The total weight of each floor is assumed 1000 kN, and the total weight of the classic and dual isolation system is 11000 kN and 12000 kN respectively. The calculated overturning moments include the P-delta forces from the large isolation layer displacements.

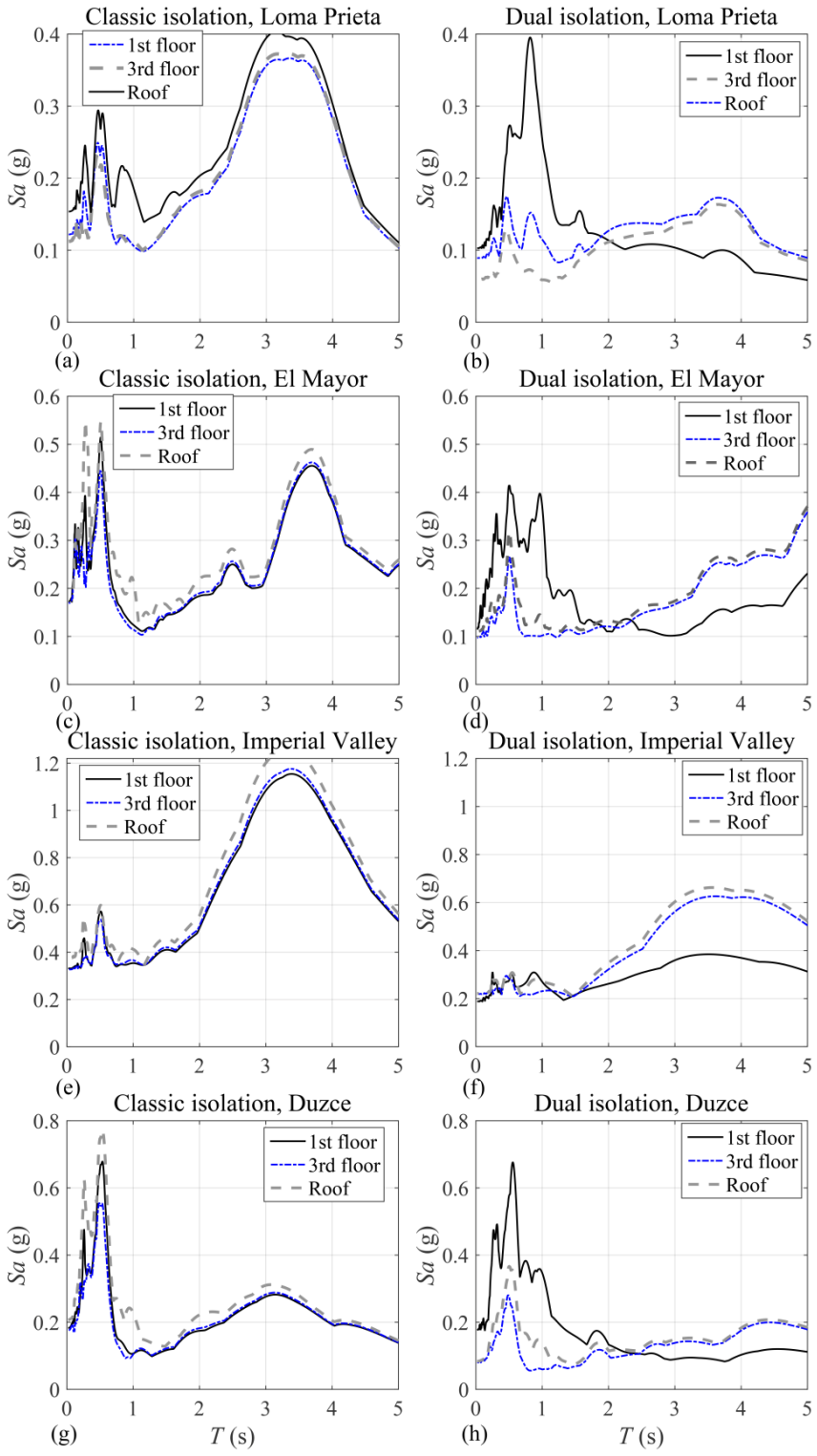

Figure 4-10: Floor response spectrum, 5% damping ratio Dual isolation: $T_1 = T_2 = 3.5$ s, $\beta_1 = 0.15$, $\beta_2 = 0.35$, $T_s = 0.9$ s, classic isolation: $T_1 = 3.5$ s, $\beta_1 = 0.15$, $T_s = 1$s.

Table 6: Base shear and overturning moment

Ground motion	Classic isolation		Dual isolation				Base moment Reduction
	V_b/W	$M_b/10e4$ $(kN.m)$	V_2/W	V_b/W	$M_2/10e4$ (kN. m)	$M_b/10e4$ (kN. m)	
Loma Prieta	0.09	2.26	0.04	0.05	1.14	1.56	31%
Kocaeli	0.14	2.90	0.06	0.07	1.31	1.92	34%
ChiChi	0.08	1.75	0.05	0.06	1.05	1.53	13%
Manjil	0.11	2.48	0.05	0.06	1.25	1.75	30%
El Mayor	0.10	2.47	0.07	0.08	2.18	2.46	0%
Imperial Valley	0.31	6.81	0.15	0.19	3.43	4.98	28%
Westmoreland	0.08	1.70	0.03	0.04	0.08	1.14	33%
Superstition	0.07	1.77	0.03	0.04	0.08	1.11	37%
Tabas	0.10	2.18	0.05	0.06	1.23	1.73	21%
Duzce	0.08	2.04	0.04	0.05	0.08	1.71	16%

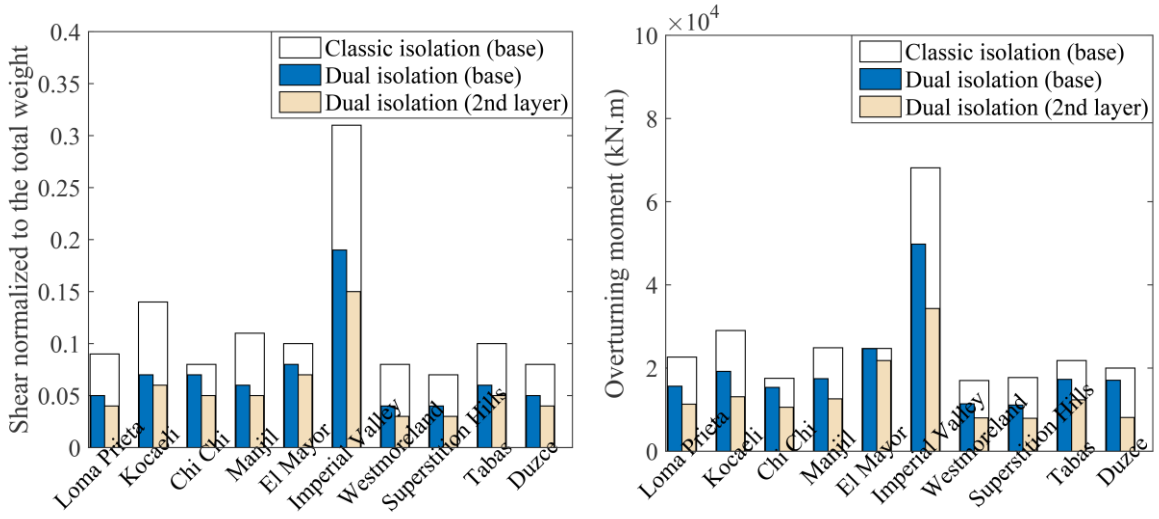

Figure 4-11: Maximum story shears and overturning moments for classic and dual Isolation systems

As expected, the maximum base shear is decreased in the dual isolation system due to the decreased displacement of the first layer compared to the displacement of the classical isolation system. Therefore, smaller member sizes and reduced cost associated to structural components are the potential benefits of this system. As an example, for the Kocaeli motion, the maximum shear at the base is 14% of the building weight in the

classic isolation system, whereas the base shear is roughly 7% of the building weight in the dual isolation system.

The maximum base overturning moment of the dual isolation system is decreased by 34% on average from classic base isolation for motions with frequency content in optimum range and 14% on average for broadband motions. This is predominantly due to the reduced accelerations in the second isolation level. Overall, the large reduction in overturning moments will aid in the design of isolation layers; however, proper consideration should be given to the overturning forces on both layers as the demands on the second layer will be of similar magnitude to those on the first.

4-2- Nonlinear Systems

In practice, lead rubber bearings (LRB) and single friction pendulum (SFP) devices are modeled by bilinear models. Three influential parameters on bilinear behaviour of these devices include initial stiffness k_1, post yield stiffness k_2, and characteristic strength Q, as shown in Fig 4-12. The initial stiffness k_1, estimated from hysteresis loops from experimental tests, or as a multiple of k_2. In practice it varies between 10 k_2 to 1000 k_2, based on the type of the isolation devices (Naeim & Kelly, 1999).

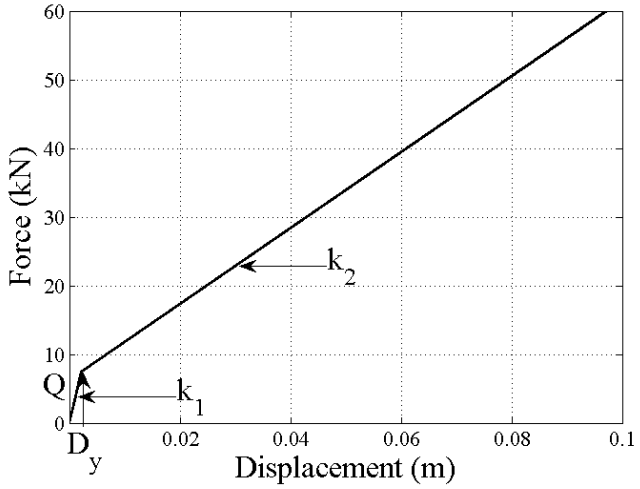

Figure 4-12: Bilinear model for isolation bearings

For LRBs the characteristic strength *Q*, depends on the yield stress and area of the lead, and post yield stiffness is the stiffness of the plain elastomeric bearing, given by the shear modulus and the thickness of the rubber, and Lastly, for FPS devices the characteristic strength is given by the coefficient of friction of the sliding surface.

The actual behaviour of LRBs and SFPs can be more accurately represented through the Bouc-Wen model, therefore a Bouc-Wen model is used to represent the hysteresis shape of the isolation layers, and the system of equation of motions is solved using the fourth and fifth order Runge-Kuttah algorithm using MATLAB ordinary differential equation solver (ode 45).

From the Bouc-Wen model the resisting force of the isolation layer is

$$F(t) = \alpha k_1 v(t) + (1-\alpha) k_1 D_y z(t) \qquad 4\text{-}1$$

where $\dot{z}$ denotes the time derivative

$$\dot{z}(t) = \frac{1}{D_y}\left(\dot{v}(t) - \gamma|\dot{v}(t)|z(t)|z|^{n-1} - \beta\dot{v}(t)|z|^n\right) \qquad 4\text{-}2$$

in which α is the ratio of post yield stiffness to initial stiffness (k_2/k_1), D_y is the yield displacement of the base isolation device, n, β and γ are the Bouc-Wen parameters that define the shape of hysteresis loops of isolation layers, and z(t) is the measure of plasticization in the model. In this study β = γ = 0.5, and n = 1. This value for n, represents a model with rounded corners for the transition between the elastic and plastic regions at the hysteresis loops.

The lateral story drifts and acceleration demands of a dual isolated system are examined and compared to its classic isolation counterpart. A ten story classic base isolated model with a moderate damping ratio β_{eff} = 0.15, and a nominal period of T_{eff} = 3.5 s is selected for the preliminary design. The design displacement of the isolation system is roughly 0.3 m, the weight on the isolation system is assumed as 1000 kN, and the 10-story superstructure building is the same as linear system.

The ASCE [5] code uses effective linear stiffness and effective viscous damping ratios to estimate the behavior of nonlinear isolation bearings;

$$T_{eff} = 2\pi\sqrt{W/k_{eff}g} \quad 4\text{-}3$$

$$\beta_{eff} = \frac{E_{loop}}{2\pi k_{eff} D^2} \quad 4\text{-}4$$

in which W is the weight on the isolator, E_{loop} is the energy dissipated in each cycle of the isolator, k_{eff} is the effective linear stiffness, and D is the maximum displacement of the isolator under the specified level of motion. The dissipated energy E_{loop}, and effective stiffness k_{eff}, are

$$E_{loop} = 4Q(D - Dy) \quad 4\text{-}5$$

$$k_{eff} = \frac{Q + (\alpha k_1 (D - Dy))}{D} \quad 4\text{-}6$$

As the behavior of the bearing is governed by two independent parameters (Q and k_1), at a target displacement, there exists a single design parameters for a specified period and effective damping ratio (Becker and Mahin, 2013) as shown in Table 7 and Fig. 4-13. Where Q_1 is the characteristic strength and α is the ratio of post yield stiffness $k_{2\text{-}1}$, to initial stiffness $k_{1\text{-}1}$ of the base isolation layer.

For comparison, a 10 story dual isolation system, with two layers of isolation at the base and first floor, following the mass ratio of 0.9, is selected to further investigate the effectiveness of the dual isolation system with bilinear behaviour. For this model, both superstructures are the same as the ones from linear system (Section 4-1).

Table 7: Preliminary design parameters of the base isolation layer

W (kN)	K_{1_1} (kN/m)	K_{2_1} (kN/m)	α	Q_1 (kN)	D_y (m)
1000	2565.5	256.5	0.10	25.63	0.01

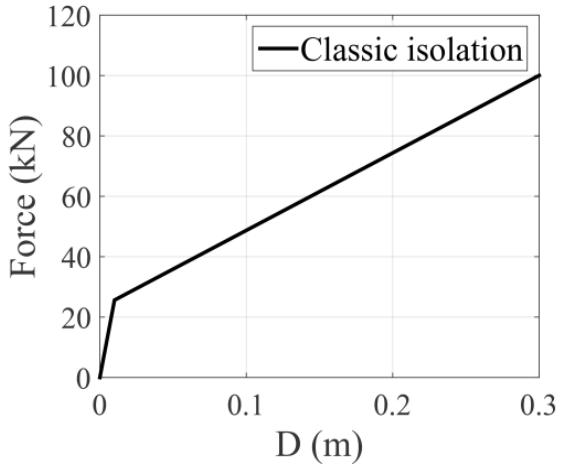

Figure 4-13: Preliminary design of classic isolation

The first isolation layer is modeled with the same design parameters as presented in Table 7, while the design parameters (Q_2, $k_{1\text{-}2}$ and $k_{2\text{-}2}$) of the second isolation system are selected based on a numerical analysis, to minimize the acceleration demands on nonstructural components of the dual isolated building. Figure 4-14 shows the average floor response spectrum of the classic isolation system under the suit of ground motions used for linear time history analysis (Table 3) .

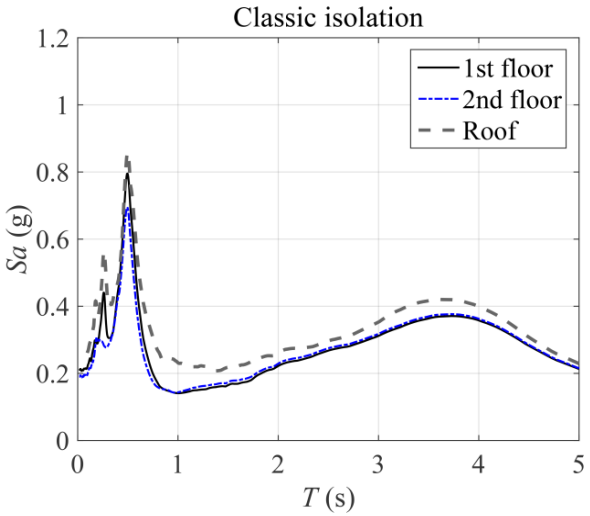

Figure 4-14: Average floor response spectrum, classic isolation, 5% damping ratio

For the classic isolation response spectra, the peak demands occur at the fundamental periods of the system: 0.25 s, 0.5 s, and 3.5 s. Varying the design parameters of the second isolation layer as shown in Fig. 4-15, the acceleration spectrum of the first floor (right above the first isolation layer), second floor (right above the second isolation layer) and roof are investigated for four different cases. These response spectra (Fig. 4-16) are compared to those from classic isolation system (Fig. 4-14) to select an optimum design for the second isolation layer.

- Case 1. Where both isolation layers have the same characteristics as shown in Table 7.
- Case 2. Where the second isolation layer has smaller characteristic strength compared to the first layer ($Q_2 = 0.5\ Q_1$).
- Case 3. Where the second isolation layer has smaller characteristic strength and initial stiffness compared to the first layer ($Q_2 = 0.5\ Q_1,\ k_{1\text{-}2} = 0.5\ k_{1\text{-}1}$).
- Case 4. Where the second isolation layer has smaller characteristic strength and smaller post yield stiffness ($Q_2 = 0.5\ Q_1, k_{2\text{-}2} = 0.5\ k_{2\text{-}1}$).

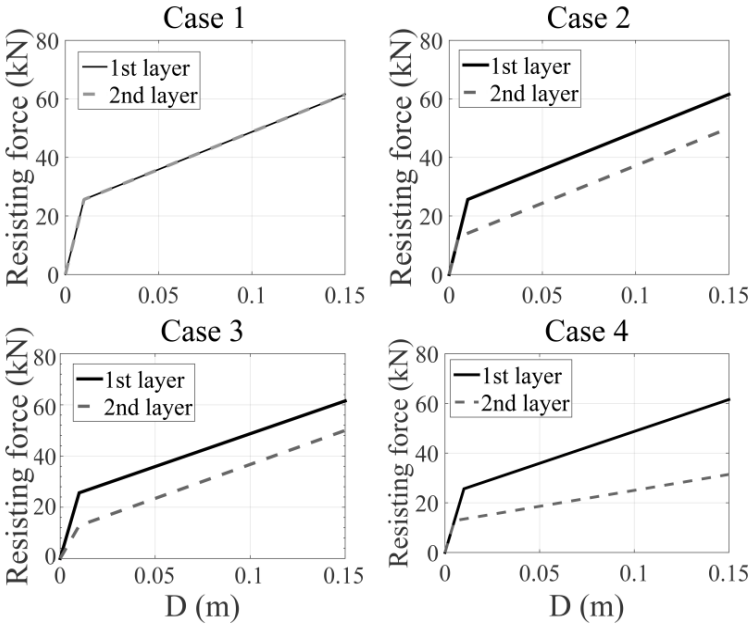

Figure 4-15: Back bone curves for different design schemes

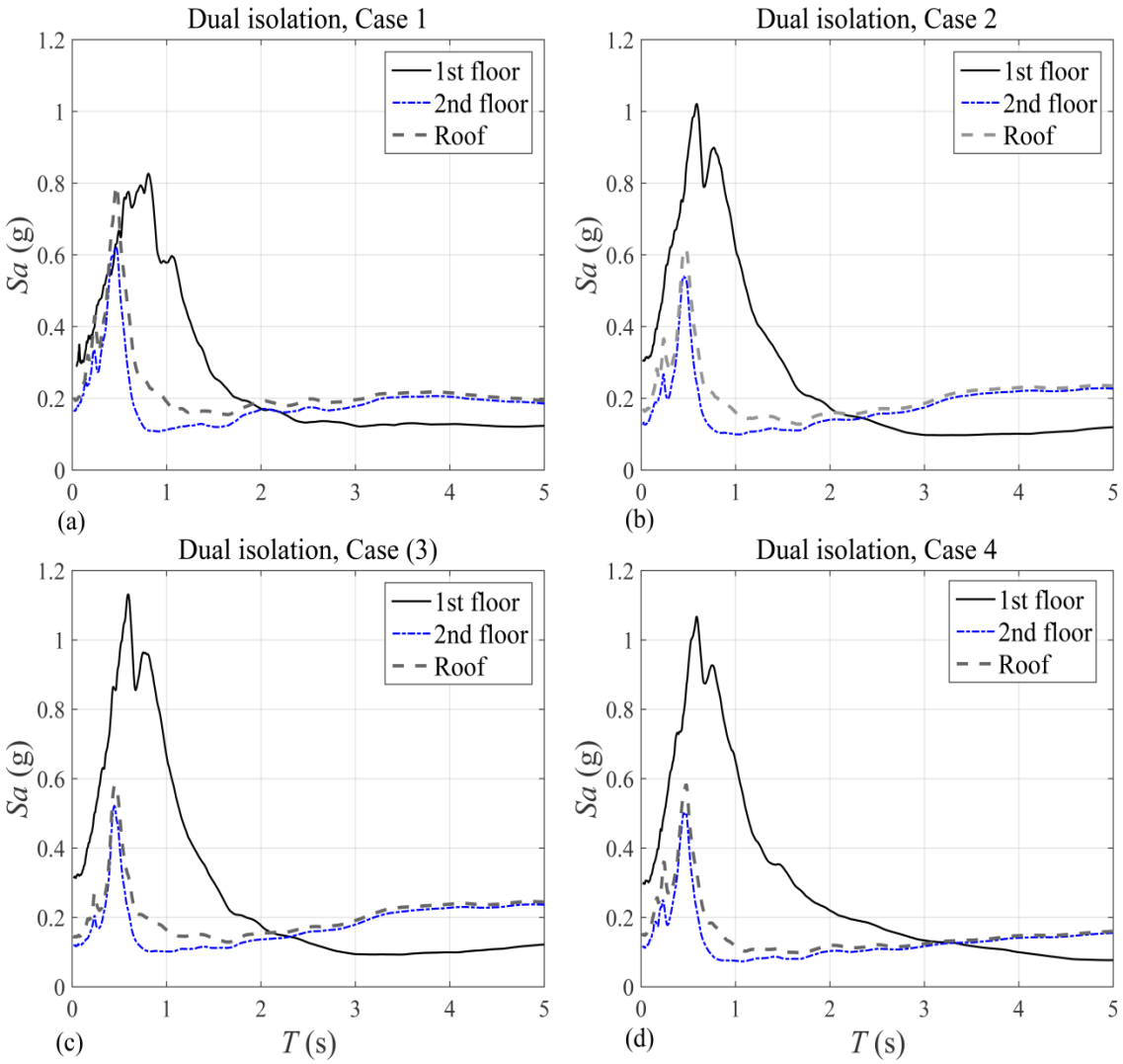

Figure 4-16: Floor response spectrum, averaged out of over 10 ground motions, 5% damping ratio. (a) Case 1, (b) Case 2, (c) Case 3, (d) Case 4

For Case 1, the acceleration demands of the first floor decrease at the period range of 3.5 s, while the demand significantly increases in 0.5 to 1 s period range close to the second and third period of the dual isolation system. For the mid-floors, the demands on systems and components are decreased, however in upper floors, the transmited accelerations in the dual isolation system are on the same order as those in the classical isolation.

For Case 2, when the second layer is designed with reduced characteristic strength, a 25% reduction on acceleration demands on the upper portion of the building are predicted at

the 0.5 s period range. As shown in Fig. 4-16 (c) and (d), the reduction in initial and postyield stiffness (Case 3 and Case 4) has minimal effect on acceleration demands.

From this numerical analysis, the second isolation layer is designed with a characteristic strength as half of the first layer, while the initial and post yield stiffness are kept as the same order as the first layer's (Table 8). This design scheme requires minimal changes in design of the second isolation layer compared to the first layer while reducing the acceleration demands on the second superstructure. The time history analysis are conducted on a model with design parameters as shown in Table 7 and Table 8.

The peak displacement and acceleration responses of the isolation layer and roof, from the classic isolation model are compared to those from the dual isolation system and shown in Table 9 and Table 10 respectively. The floor acceleration and absolute displacement time histories are shown in Fig. 4-17 and Fig. 4-18 for Loma Prieta and El Mayor as an example of broadband motions, and in Fig. 4-19 and Fig. 4-20 for Imperial Valley and Duzce, as an example of pulse-type ground motions. In addition the maximum interstory drifts and peak floor accelerations are shown in Fig. 4-21 over the height of the building.

Compared to the classic isolation system, the addition of the mid-isolation layer decreases the relative base displacement of the dual isolation $v_{1,}$ for both pulse and non-pulse type motions by up to 54%, However, the total displacement of the second isolation layer u_2, and roof u_{10}, is increased by 21% and 18% on average.

Table 8: Preliminary design parameters of the second isolation layer

W (kN)	K_{1_2} (kN/m)	K_{2_2} (kN/m)	α	Q_1 (kN)	D_y (m)
900	2565.5	256.5	0.10	12.32	0.005

Table 9: Peak floor displacement, bilinear behaviour

Ground motion	Classic Base Isolation		Dual Isolation		
	u_1 (m)	u_{10} (m)	u_1 (m)	u_2(m)	u_{10} (m)
Loma Prieta	0.29	0.33	0.16	0.29	0.31
Kocaeli	0.42	0.46	0.27	0.56	0.58
Chi Chi	0.16	0.18	0.14	0.30	0.32
Manjil	0.34	0.37	0.20	0.38	0.39
El Mayor	0.27	0.30	0.24	0.49	0.50
Imperial Valley	1.36	1.48	0.65	1.36	1.42
Westmorland	0.22	0.24	0.11	0.25	0.25
Superstition Hills	0.22	0.25	0.10	0.21	0.23
Tabas	0.34	0.36	0.20	0.40	0.42
Duzce	0.19	0.22	0.09	0.20	0.22

Table 10: Peak floor acceleration, bilinear behaviour

Ground motion	Classic Base Isolation		Dual Isolation		
	A_1 (g)	A_{10} (g)	A_1 (g)	A_2 (g)	A_{10} (g)
Loma Prieta	0.18	0.19	0.28	0.12	0.14
Kocaeli	0.21	0.25	0.35	0.14	0.18
Chi Chi	0.22	0.24	0.35	0.13	0.14
Manjil	0.18	0.24	0.29	0.16	0.17
El Mayor	0.18	0.18	0.35	0.12	0.13
Imperial Valley	0.41	0.43	0.32	0.25	0.27
Westmorland	0.16	0.16	0.14	0.10	0.11
Superstition Hills	0.18	0.18	0.32	0.09	0.13
Tabas	0.25	0.27	0.28	0.15	0.18
Duzce	0.21	0.27	0.35	0.14	0.17

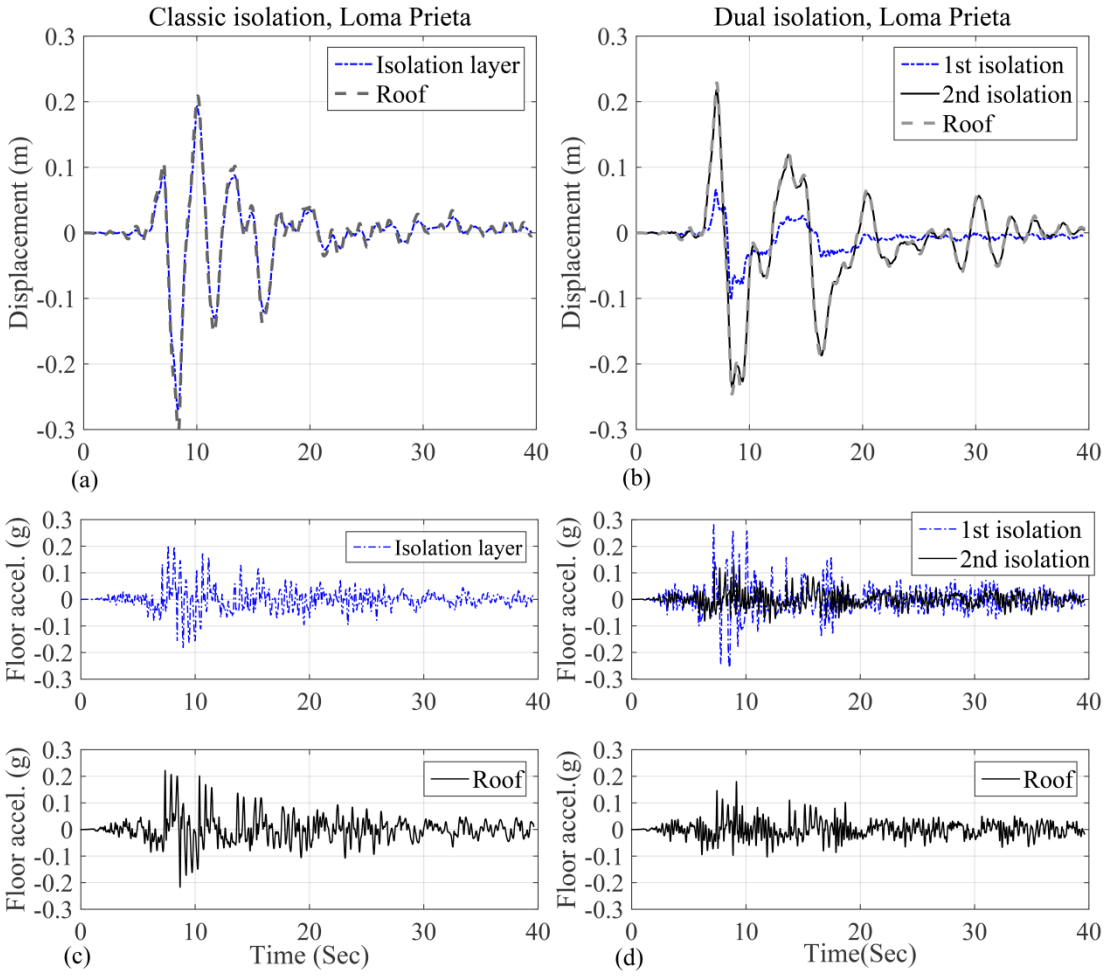

Figure 4-17: Time history analysis, Loma Prieta, (a) classic isolation, displacement, (b) dual isolation, displacement, (c) classic isolation, acceleration, (d) dual isolation, acceleration

The average reduction in displacements of first isolation layer from both linear and nonlinear analysis is roughly 40% compared to the classical system. However the total roof displacement is slightly higher in nonlinear analysis (18% compared to 13%) which can be a result of differences between damping ratio of the second isolation layer in the linear and bilinear models.

As discussed in Section 4-1, the efficiency of the dual isolation system depends on the frequency content of the ground motion. The total roof displacement is greater for ground motions which have more energy in higher frequency content such as Chi Chi, El Mayor

and Manjil, however; it is as the same order as the displacement in classical system for motions with lower frequency content. This deduction is not consistent for Kocaeli motion; while the maximum roof displacement of the dual isolation from linear analysis is on the same order as the classic isolation system, the total displacement from nonlinear analysis is increased by 33% (compared to classic isolation).

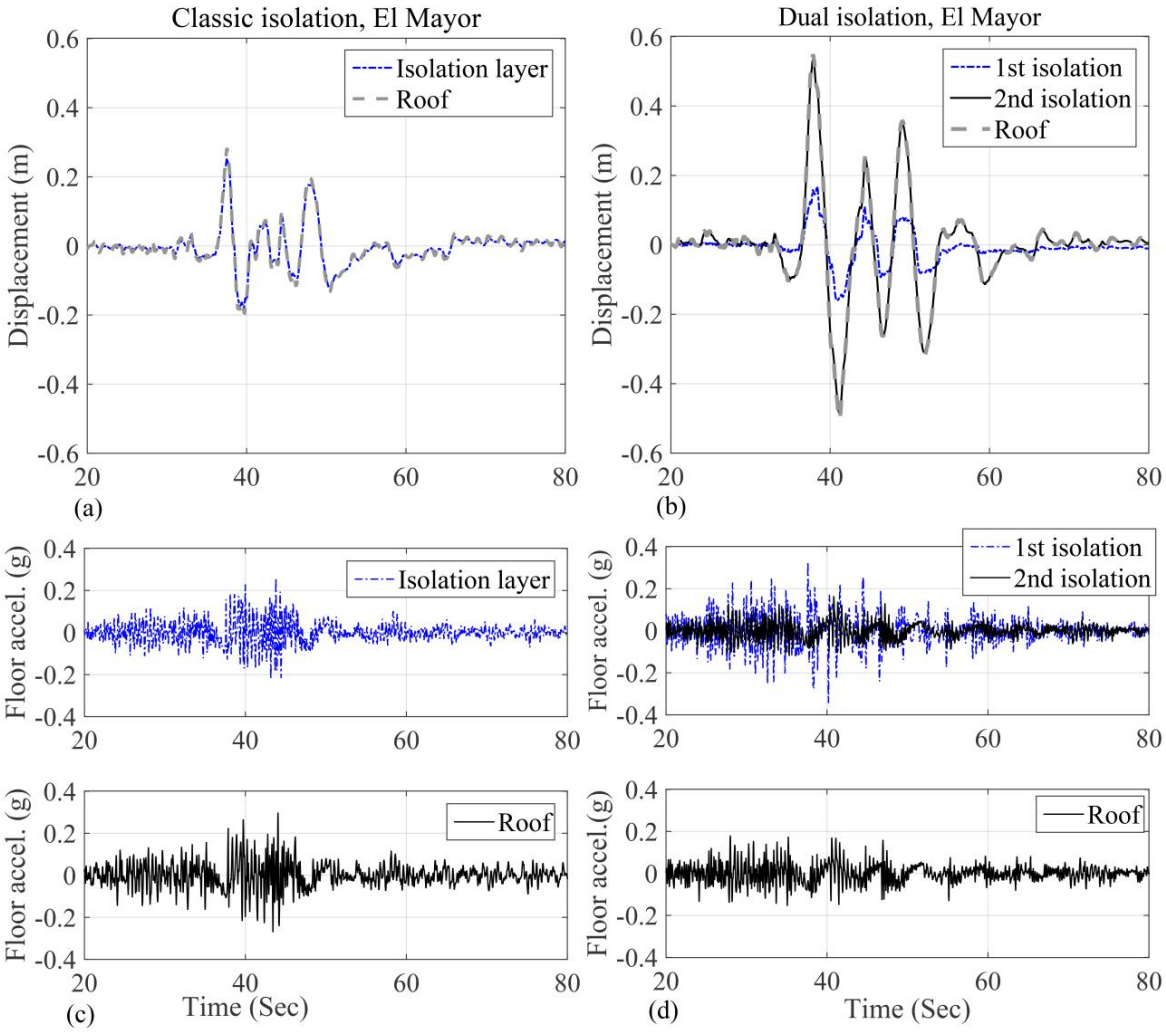

Figure 4-18: Time history analysis, El Mayor, (a) classic isolation, displacement, (b) dual isolation displacement, (c) classic isolation, acceleration, (d) Dual Isolation, acceleration

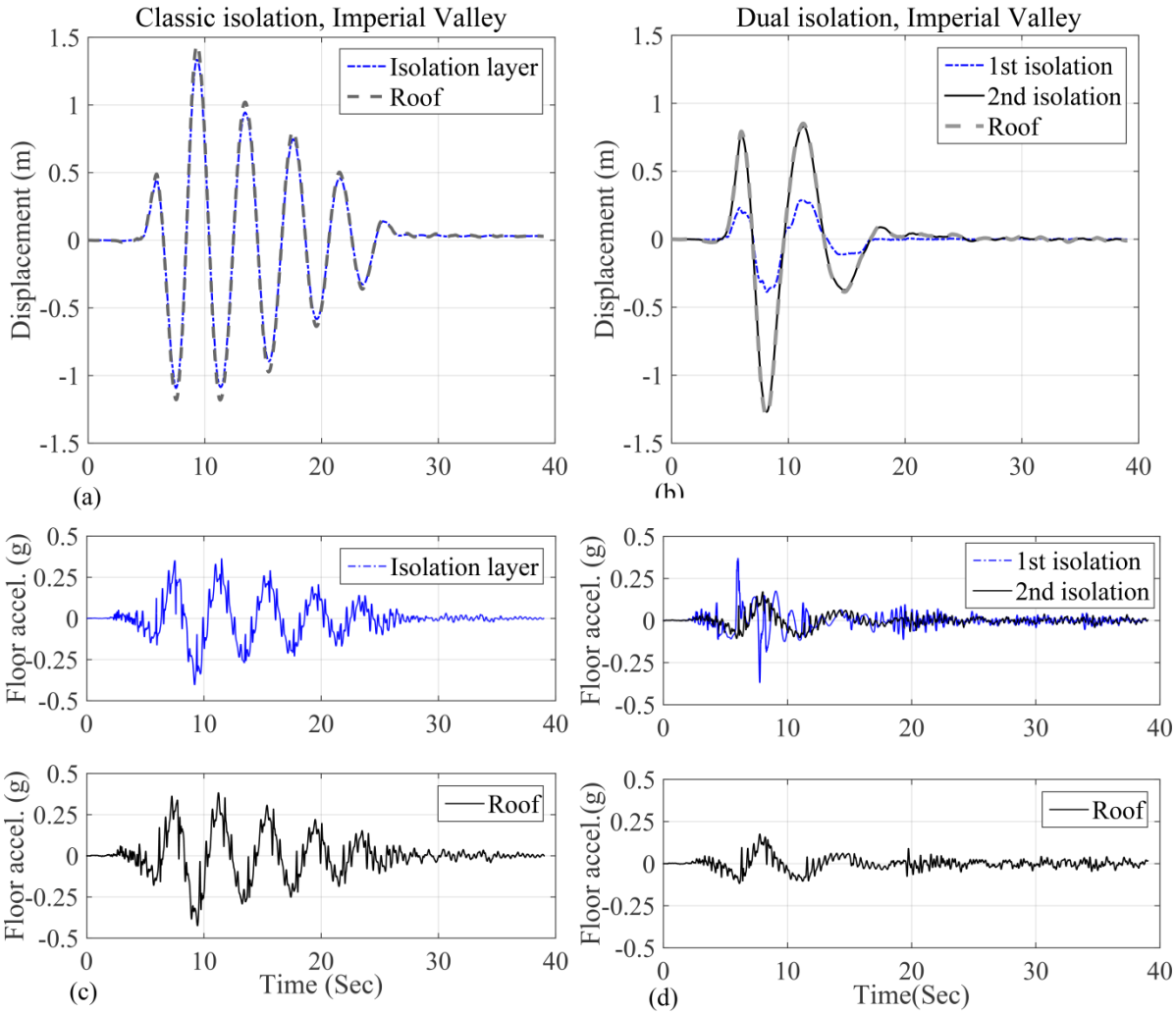

Figure 4-19: Time history analysis, Imperial Valley, (a) classic isolation, displacement, (b) dual isolation displacement, (c) classic isolation acceleration, (d) dual isolation acceleration

As shown in Fig. 4-21, the peak acceleration in the second isolation layer decreases for all ground motions by 30% on average. This reduction is roughly constant over the height of the building, ie., a 26% reduction in mid-height and roof level.

In the dual isolation system with nonlinear devices, significantly larger acceleration is transmitted to the first isolation layer and its superstructure, although this increase in acceleration demand on the first isolation layer was observed from linear analysis, this index is higher when the bilinear models are used for time history analysis.

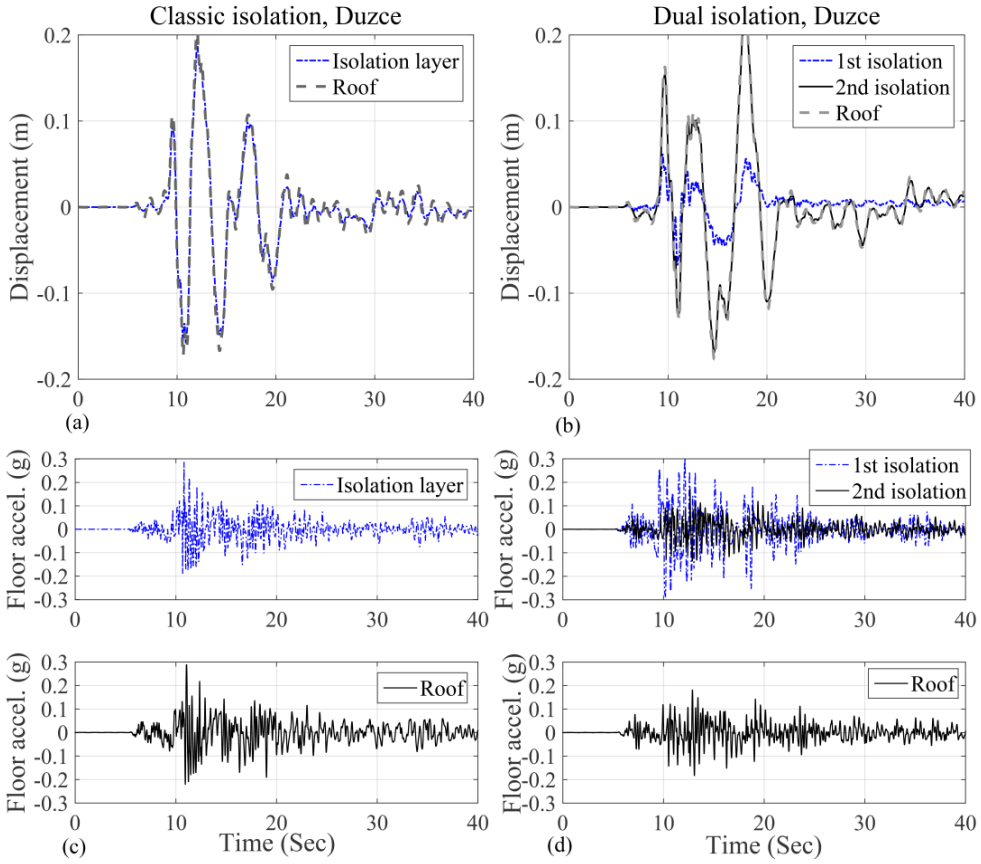

Figure 4-20: Time history analysis, Duzce, (a) classic isolation, displacement, (b) dual isolation displacement, (c) classic isolation acceleration, (d) dual isolation acceleration

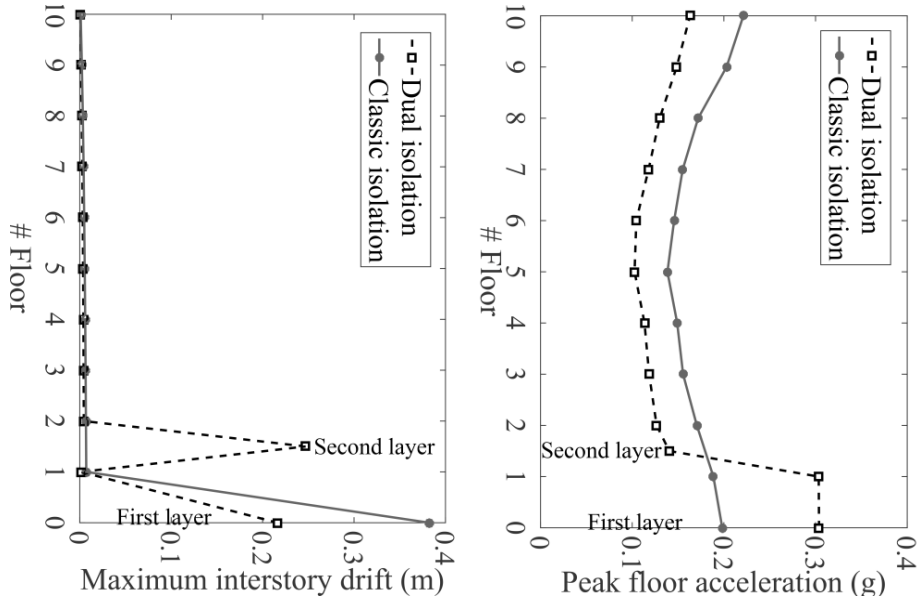

Figure 4-21: Maximum Interstory Drifts and Peak Floor Accelerations, Average of 10 Motions

4-3- Dual Isolation for Multiple Hazard Levels

The purpose of this section is to design a system that behaves more like a dual isolation under Maximum Considered Earthquakes (MCE), and yet behaves as a classic isolation system when the building is excited by Design Bases Earthquakes (DBE) which have higher probability of occurrence. This system avoids exceeding displacements in large earthquakes, while providing isolation effects under design level events. A two DOF dual isolation system with mass ratio $\gamma = 0.9$ is considered for this analysis, the design parameters of the first isolation layer are shown in Table 7. The characteristic strength and initial stiffness of the upper isolation layer is chosen so that the second layer will not yield at the DBE design displacement force. Figure 4-22 shows the bilinear model of the proposed dual isolation system. The characteristic strength of the second layer $Q_{2,}$ is roughly four times greater than the characteristic strength of the first layer Q_1, and the initial stiffness of the second layer k_1-$_2$ is three times larger than the initial stiffness of the first layer, k_1-$_1$.

The absolute displacement and acceleration time histories of the proposed dual isolation system are shown in Fig. 4-23 for the Loma Prieta and Chi Chi ground motions to represent the behaviour of this system under design base events. It is shown that the second isolation layer does not contribute to lateral displacement of the system. Although, the model behaves roughly as a classic isolation system, the second isolation layer has unfavorable influence on acceleration history of the base.

Two ground motions scaled to the MCE spectrum (Fig. 4-24) are selected to examine the behaviour of the system under MCE hazard level. The specifications of these motions are presented in Table 11. A single DOF classical isolation with isolation design parameters as shown in Table 7 is used to compare the time history results to those from the dual isolation.

Table 11: Selected ground motions, MCE level

#	NGA Record #	Earthquake	Year	Station	Scale Factor	Pulse Period
1	183	Imperial Valley	1979	El Centro Array # 8	1.62	-
2	1115	Kobe	1995	Sakai	3.20	-

From nonlinear analysis (Section 4-2), the average reduction in base displacement and floor accelerations were roughly 40% and 25% respectively for a dual isolation system designed for DBE level. The behaviour of the proposed system under multiple hazards is shown in Fig. 4-25 and Fig. 4-26 for Imperial Valley and Kobe ground motions. For Imperial Valley (Fig. 4-25), the maximum displacement of the base in the dual isolation system is decreased from 0.6 m to 0.5 m (17% decrease) and the total roof displacement is on the same order as the classic isolation system, however; the system is not successful in reducing the floor acceleration above the second isolation layer. Therefore, this system has lower efficiency than the dual isolation system which is designed for a specific hazard level.

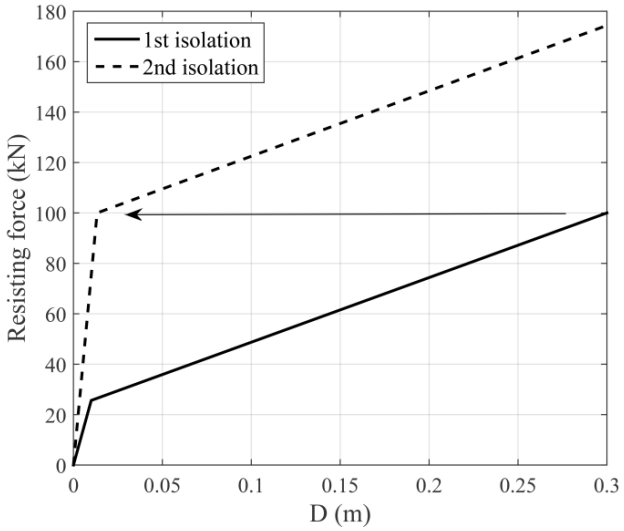

Figure 4-22: Design of dual isolation system for multiple hazard level

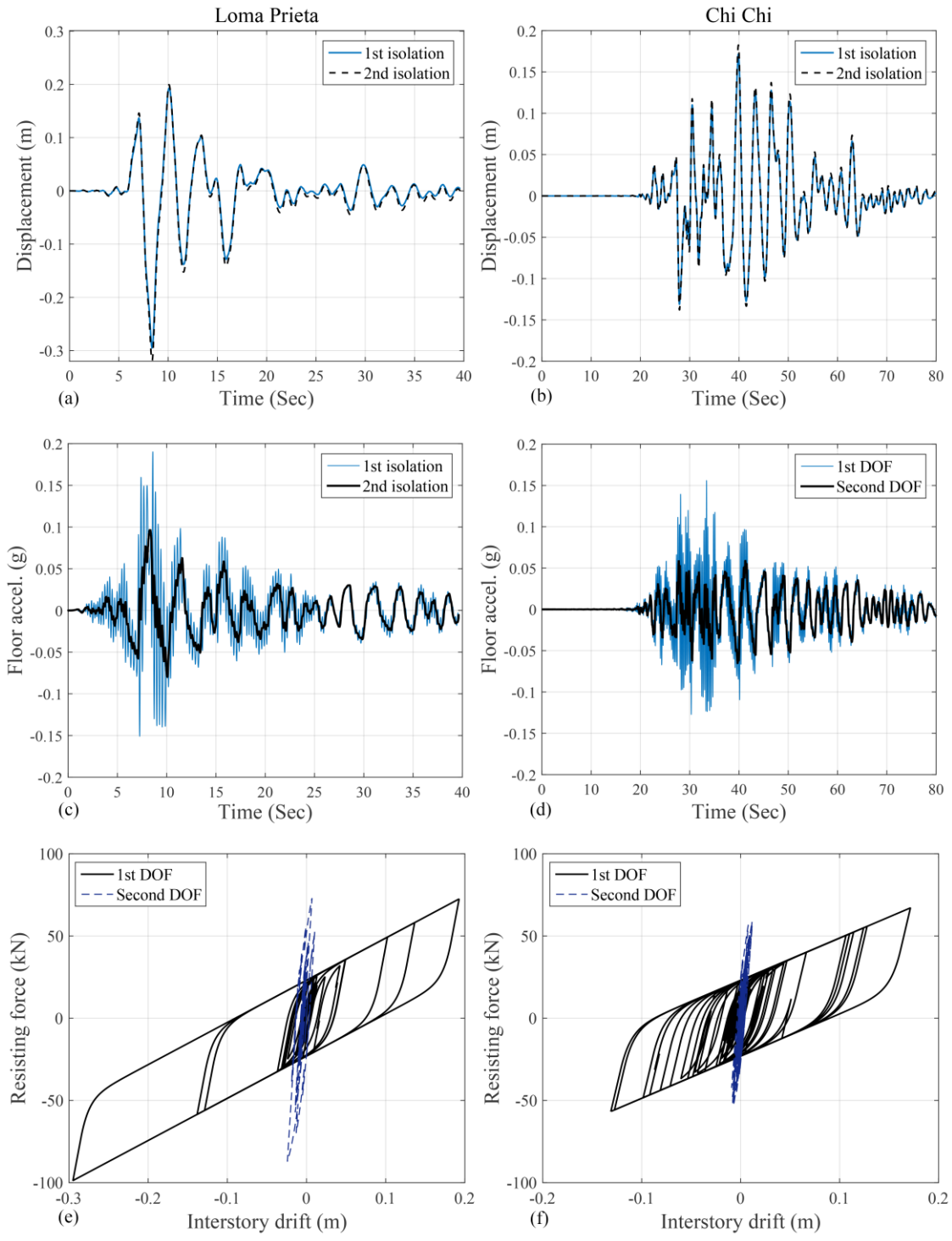

Figure 4-23: Time history results of the dual isolation model when the system is designed to behave as classic isolation. (a) Loma Prieta, displacement, (b) Chi Chi, displacement, (c) Loma Prieta, acceleration, (d) Chi Chi, acceleration, (e) Loma Prieta isolation hysteresis, (f) Chi Chi isolation hysteresis.

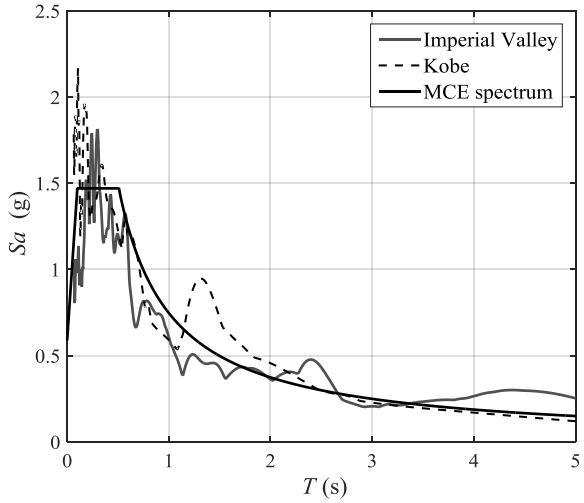

Figure 4-24: Ground motions response spectrum scaled to MCE level, 5% damping ratio

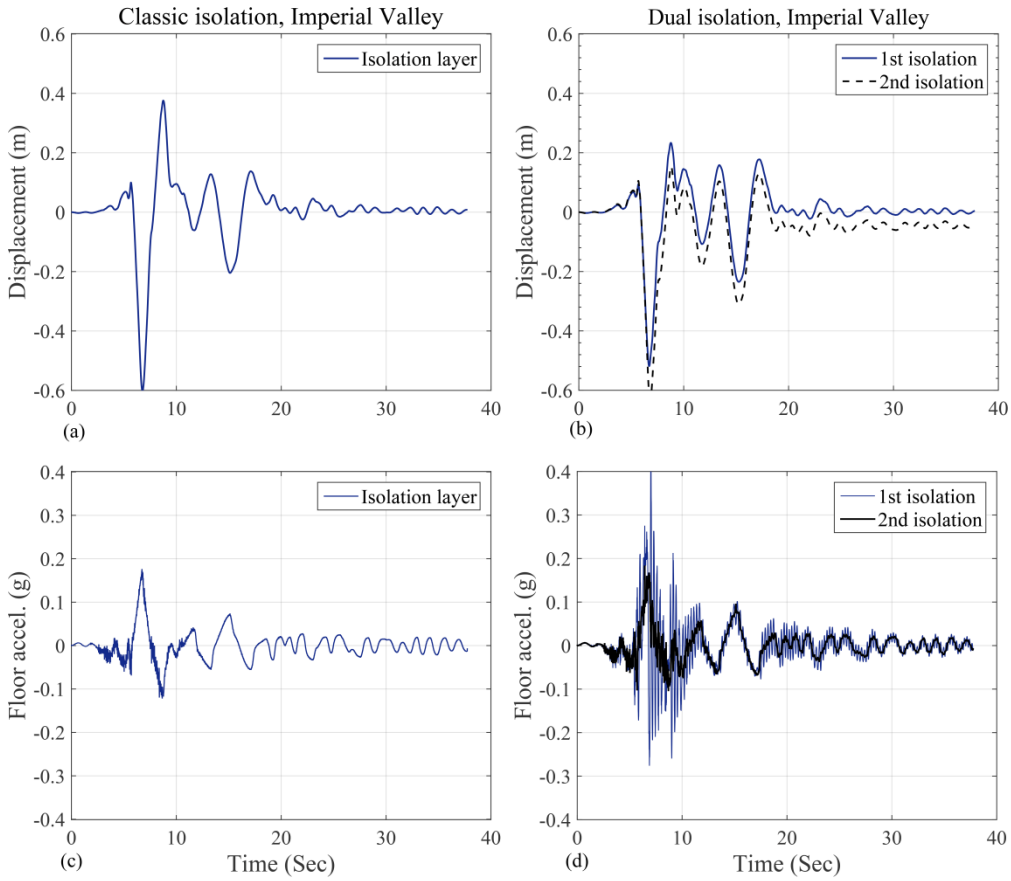

Figure 4-25: Time history analysis, Imperial Valley

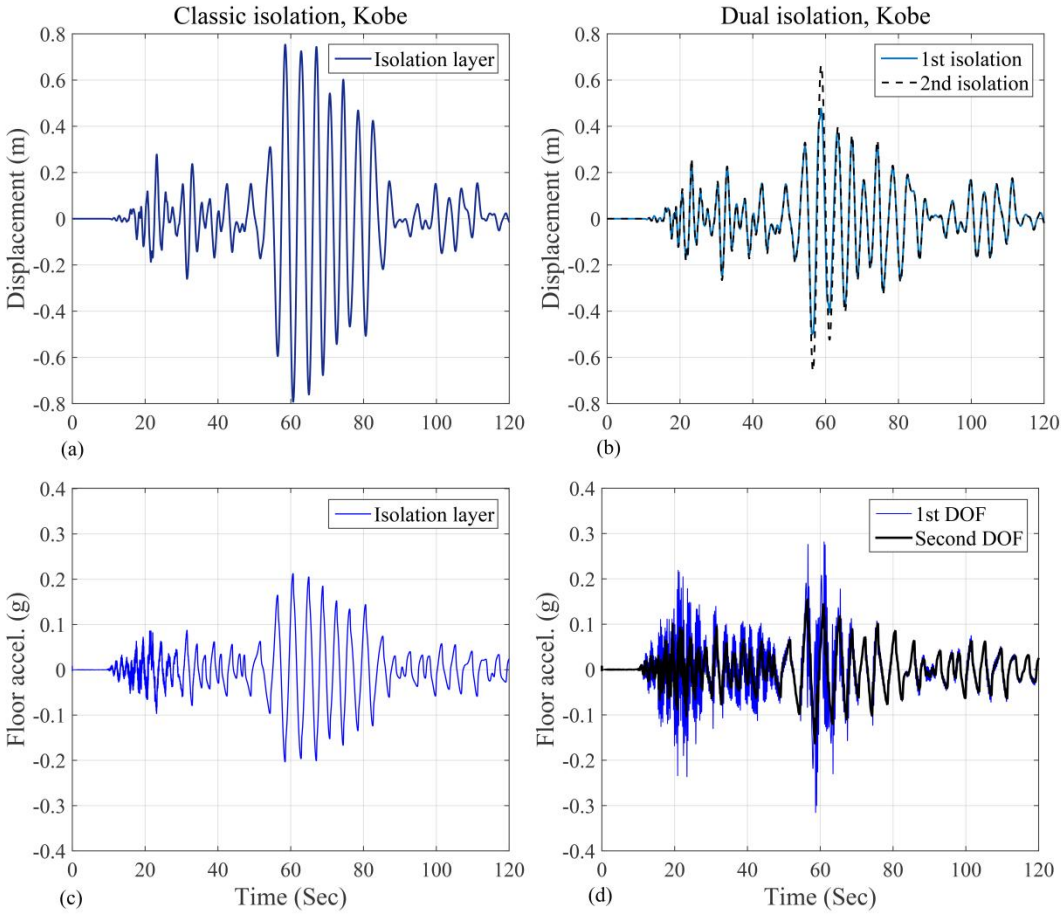

Figure 4-26: Time history analysis, Kobe

For the Kobe motion (Fig 4-26), the base and the roof displacement of the classic isolation system is reduced by 44% and 20% respectively while the peak accelerations on upper floors are roughly decreased by 15%. Therefore, the design strategy successfully avoids large displacements of the base under a motion scaled to MCE level. It can be seen in Fig. 4-27 that the second isolation layer was not fully activated during the Imperial Valley motion, therefore it was not effective in reducing the response parameters of the classic system. However, more studies are required to validate the behaviour of dual isolation systems under multiple seismic hazard levels and to optimize the systems characteristics.

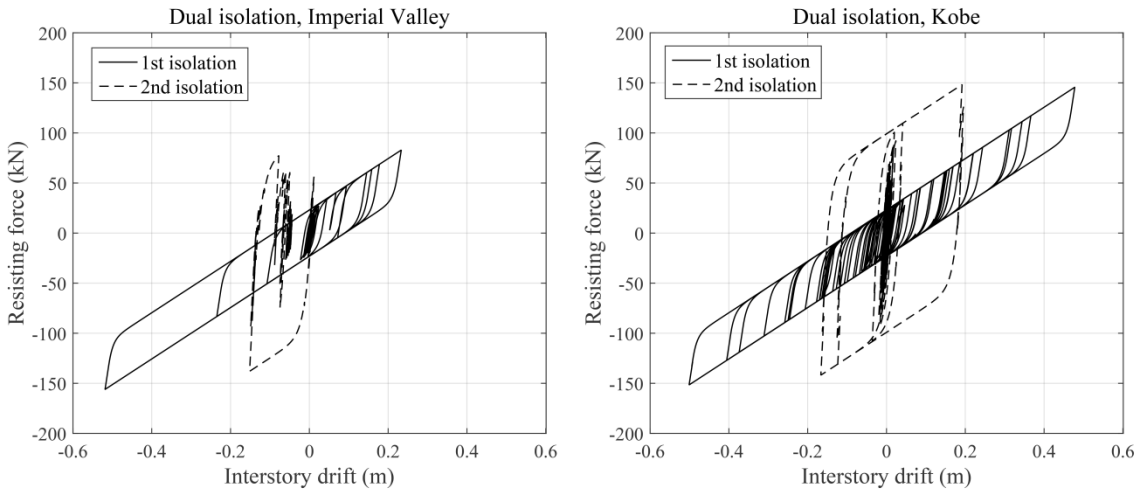

Figure 4-27: Dual isolation, isolation hysteresis. (Left): Imperial Valley, (Right): Kobe

5- Conclusion

In this study, an innovative isolation configuration, dual isolation, with two layers of isolation, at the base and mid-story, was proposed and investigated. The application of the dual isolation system was studied using a two degree of freedom model, assuming rigid body behaviour for the superstructures. From this study the ratio of the frequencies of the two isolation systems was selected to be one similar to the tuned mass dampers. However, unlike TMD, the displacement of the second isolation layer was of concern, and a larger mass ratio γ, was found to be beneficial for the reduction of displacement for both degrees of freedom, and a mass ratio of 0.9 was selected. This could represent a ten story building with isolation layers located at the base and at the top of the first floor. It was shown that a low to moderate damping ratio for the first isolation layer and a larger damping ratio for the second isolation layer improve the displacement behaviour of the system.

A ten story dual isolation system with linear isolation devices, following the mass ratio of 0.9 was analyzed under ten scaled ground motions with varying frequency content, including five pulse types and five broadband records, to investigate drifts and accelerations. The adoption of the second isolation layer reduced the lateral displacement of the first layer by up to 50% compared to traditional base isolation. The displacement of the roof is increased by 13% on average. The dual isolation system increased acceleration in the non-structural content frequency range below the second isolation layer. However, it decreased the peak floor acceleration in the second layer and the upper superstructure (which represents the majority of the building floor area) by 40% on average compared to its base isolation counterpart. Large reductions are also seen in floor response spectra over the frequency range associated with building systems and components. This reduction increases occupants' safety, reduces the damage to non-structural components and enhances the building's capability to remain fully operational after earthquake. In

addition, this decreased acceleration limited the overturning moments that cause uplift and can be harmful to isolators.

Frequency analysis was used to examine the robustness of the dual isolation system to diverse ground motions by looking at the behaviour at stiff, medium, and soft soil sites. Results show that the dual isolation system is good for all soil types, however it is marginally more effective in reducing the displacement demand on the first floor in softer soil conditions. This is in line with the findings from time history analysis; the proposed system is most effective in reducing the displacement and acceleration responses (compared to a classic base isolated building) under excitations with frequency content closer to that of the isolation system, in the 0.3 to 1 Hz range.

The effect of bilinear isolation systems on dual isolation was then investigated. The first isolation layer was designed for a design basis earthquake with a moderate damping ratio $\beta = 0.15$, and a nominal period $T = 3.5$ s, the same as the first isolation layer in the linear model. A time history analysis was used to select the design parameters of the second isolation layer when the acceleration demands on the system were minimized. From this analysis, the characteristic strength of the second layer is selected as half of the first layer, while the initial and post yield stiffness are set as the same order as the ones from the first isolation. The findings showed a significant increase in the acceleration demand below the second isolation, however; the floor accelerations transmitted to the upper superstructure were decreased by roughly 25% while the base displacement was decreased by up to 52% (compared to classic base isolated building). The roof displacement was increased by 18% on average with the concession that the dual isolation system was more effective for the ground motions with lower frequency content.

The numerical time history analysis of the dual isolation system with bilinear behaviour is in line with the results of the linear analysis; The base displacement and peak floor accelerations were reduced in both linear and bilinear models, whereas, the acceleration demand on system and components located below the second isolation were significantly larger in the bilinear model compared to the linear analysis.

Due to the successful role of the dual isolation system in reducing responses under ground motion excitations, this system can be effectively implemented to address particular design needs. However, more studies can be done to further examine and optimize the system's behaviour and examine the associated cost with the dual isolation compared to classic isolation system.

Reference

ASCE/ SEI 7-10. (2010). *Minimum design loads for buildings and other structures.* American Society of Civil Engineers.

Becker, T., and Mahin, S. (2012). Experimental and analytical study of the bi directional behavior of the triple friction pendulum isolator. *Journal of Earthquake Engineering and Strucural Dynamics,* 41(3), 355-373.

Becker, T., and Mahin, S. (2013). Approximating peak response in seismically isolated buildings using generalized modal analysis. *Journal of Earthquake Engineering and Structural Dynamics,* 1807-1825. doi: 10.1002/eqe.2299.

Chen, G., and Wu, J. (2001). Optimal placement of multiple tuned mass dampers for seismic structures. *Journal of Structural Engineering,* 127(9), 1045-1053.

Chien Pan, T., and Cui, W. (1998). Response of segmental buildings to random seismic motions. *ISET Jurnal of Earthquake Technology*, 35(4), 105-112.

Chien Pan, T., Fu Ling, S., and Cui, W. (1995). Seismic response of segmental buildings. *Journal of Earthquake Engineering and Structural Dynamics,* 24(7), 1039-1048.

Chopra, A. (2001). Dynamics of structures, theory and application to earthquake engineering. *Prentice Hall*, London.

Chowdhury, A., and Iwuchnkwu, M. (1987). The past and future of seismic effectiveness of tuned mass dampers. *2nd International Symposium of Structural Control, H. H. E. Leipholz, ed., Martinus Nijhoff Publishers.* Hague, Netherlands.

Clark, A. (1988). 'Multiple passive tuned mass dampers for reducing earthquake induced building motion. *9th World Conference of Earthquake Engineering,* Vol.V, 779-784, Kyoto, Japan.

Crandall, M., and Mark, W. (1963). Random vibration in mechanical systems. *Academic Press*, New York and London.

Der Kiureghian, A. (1981). A response spectrum method for randon vibration analysis of MDF systems. *Journal of Earthquake Engineering and Structural Dynamics, 9*, 419-435.

Der Kiureghian, A. (1996). A coherency model for spatially varying ground motions. *Journal of Earthquake Engineering and Structural Dynamics, 25*(1), 99-111.

Dutta, A., Sumincht, J., Mayes, R., Hamburger, R., and Citipitioglu, A. (2008). An innovative application of base isolation technology. *18th Analysis and Computation Specialty Conference, ASCE Structures Congress* (pp. 18-20). Vancouver, BC, Canada.

Elangi, I. (2008). Earthquake protection of buildings by seismic isolation. *Young Researchers Conference.*

Hoang, N., Fujino, Y., and Warnitchai, P. (2008). Optimal tuned mass damper for seismic applications and practical design formulas. *Journal of Engineering Structures,* 30(3), 707-715.

Jangid, R., and Kelly, J. (2001). Base isolation for near fault motions. Journal of *Earhquake Engineering and Structural Dynamics*, *30*, 691-707.

Kanai, K. (1957). Semi-empirical formula for the seismic characteristics of the ground. *Bulletin of the Earthquake Research Institute,* The University of Tokyo.

Kelly, J. (1982). The influence of base isolation on the seismic response of light secondary equipment. *Earthquake Engineering Research Centre (EERI).*

Kelly, J. (1999). The role of damping in seismic isolation. *Journal of Earthquake Engineering and Structural Dynamics,* 28(1), 3-20.

Kelly, T. (2001). Base isolation of the structures, Design Guidelines. *Holmes Consulting Group Ltd*.

Kidokora, R. (2008). Self Mass Damper (SMD), Seismic control system inspired by the pendulum movement of an antique clock. *The 14th World Conference on Earthquake Engineering.* Beijing, China.

Matta, E. (2012). Effectiveness of tuned mass dampers against ground motion pulses. *Journal of Structural Engineering*, 139(2), 188-198.

Naeim, F., and Kelly, J. (1999). Design of Seismic Isolated Structures. *John Wiley & Sons, Inc.*

Palazzo, B., and Petti, L. (1999). Combined control strategy: Base isolation and tuned mass damper. *ISET Journal of Earthquake Technology, 36*, 121-137.

Ryan, K., and Earl, C. (2010). Analysis and Design of Inter-Story Isolation Systems with Nonlinear Devices. *Journal of Earthquake Engineering, 14*, 1044-1062.

Reinoso, E., and Miranda, E. (2005). Estimation of floor acceleration demands in high-rise buildings during earthquake. *The Structural Design of Tall and Special Buildings, 140*, 107-130.

Sadek, F., Mohraz, B., Taylor, A., and Chung, R. (1997). A method of estimating the parameters of tuned mass dampers for seismic application. *Journal of Earthquake Engineering and Structural Control, 26*(6), 617-636.

Sakamoto, I. (1978). Seismic performance of nonstructural and secondary structural elements. *University of California, Earthquake Engineering Research Center*.

Sladek, J., and Klinger, R. (1983). Effect of tuned-mass dampers on seismic response. *Journal of Structural Engineering, 109(8)*, 2004-2009.

Tajimi, H. (1960). A statistical method of determining the maximum response of a building structure during an earthquake. *2nd world Conference on Earthquake Engineering, Vol. II.*

Taniguchi, T., Der Kiureghian, A., and Melkumyan, M. (2008). Effect of tuned mass damper on displacement demand of base-isolated structures. *Journal of Engineering Structures, 30*(12), 3478-3488.

Tsuneki, Y., Torii, S., Murakami, K., and Sueoka, T. (2008). Middle-story isolated structural system of high-rise building. *The 14th Word Conference on Earthquake Engineering*, Beijing, China.

Wolff, E., Ipek, C., Constantinou, M., and Tapan, M. (2014). Effect of viscous damping devices on the response of seismically isolated structures. *Journal of Earthquake Engineering and Structural Dynamics*, 44 (2), 185-198.